MEASUREMENT OF INTERDIFFUSION IN THE SYSTEM Mn_xO-MgO BY NEUTRON ACTIVATION ANALYSIS

by

Roger Montrose Conant

A Thesis Submitted to the
Graduate Faculty in Partial Fulfillment of
The Requirements for the Degree of
MASTER OF SCIENCE

Major Subject: Nuclear Engineering

Approved:

Iowa State University
Of Science and Technology
Ames, Iowa

1970

TABLE OF CONTENTS

TABLE OF FIGURES

I. INTRODUCTION

The study of diffusion in single crystals of magnesium oxide is very important since many properties of magnesium oxide are dependent on the impurities which may have diffused into the crystal. Sinterability, ionic conductivity, creep, optical, electrical, melting point, and oxidation and reaction rates are all examples of properties or processes in magnesium oxide for which diffusion of ions may be the rate-determining process.

The properties of interest to the High Temperature Ceramic Groups of Project Themis are the ionic conductivity and high temperature creep mechanisms of single crystals of magnesium oxide. Of major importance to the high temperature creep study group is the effect of MnO diffusion into the single crystal magnesium oxide on its creep resistance.

The purpose of this study is to explore the application of neutron activation analysis to the study of interdiffusion by measuring the amount of manganese which diffuses into the magnesium oxide and subsequently to determine the interdiffusion coefficient for the system Mn_xO-MgO. Diffusion rates have been measured by radioactive tracer techniques, chemical analysis, and microprobe analysis. The technique which is being applied in this work is neutron activation analysis.

II. REVIEW OF THE LITERATURE

A. Activation Analysis

Activation analysis had its beginning in the papers of Hevesy and Levi in 1936 (1) and Seaborg and Livingood in 1938 (2). During the first ten years of activation analysis, less than 24 papers were published, but beginning in 1949 when 13 papers were published, the annual rate of growth increased to almost 600 in 1967.

An excellent bibliography (3) has been compiled on activation analysis. This bibliography covers the whole scope of activation analysis from the work of Hevesy and Levi up through 1969. The bibliography indexes activation analysis by author, element analyzed, matrix analyzed, and technique applied. The compilation by Roberts, Whitmer, and Nieman (4) is also an excellent bibliography. Another very good work for reference purposes is the book by Koch (5), which goes into some detail on the history and growth of activation analysis, the general technique of activation analysis, some theoretical consideration of activation analysis, a tabulation of nuclear data, experimental methods, evaluation of nuclear reactions, standard sensitivities, and references.

The books by Lenihan and Thomson (6), and Lyon (7) are rather elementary but useful monographs on activation analysis.

Several state-of-the-art conferences on activation analysis have been held including the International Conferences on

Modern Trends in Activation Analysis (8, 9, 10, and 11) and the Radioactivation Analysis Symposium held in Vienna, Austria, in June, 1959 (12). The proceedings of these conferences are important sources of information on a wide range of topics.

Many investigators have applied neutron activation analysis in the determination of manganese in different materials. Among these investigators are Voigt and Abu-Samra (13) who determined the manganese concentration in a sword made from Damascus steel; Kawashima (14) who determined the manganese concentration in samples of niobium and tantalum; Rojas, Dyer, and Cassatt (15) who determined the concentration of manganese in bone; Bate and Dyer (16) who determined manganese in human hair; and Romberg (17) and Lee (18) who have determined the manganese concentration in single crystal magnesium oxide (the matrix material involved in this study). Of course, many other manganese determinations in different materials have been reported but the above list of references serves to show the varied materials in which manganese has been determined by neutron activation analysis.

There has been very little written on the use of neutron activation analysis as applied to diffusion. The possible use of neutron activation analysis as a tool in determining diffusion coefficients was introduced by Ryskin (19) in 1959, although the author apparently has not yet performed any experimental work.

Leliaert (20) carried out studies for the determination of trace element diffusion in quartz and in germanium. The work did not deal with any determination of the diffusion coefficients but only with the distribution of trace elements in quartz and germanium.

Ascoli and Germagnoli (21) applied neutron activation analysis in the determination of interdiffusion in the system gold-lead using a technique which is probably rather similar to that employed in this study.

B. Diffusion

Since diffusion in an oxide matrix is of interest in this study, diffusion in oxides will be of primary concern in this literature review. Even though this narrows the diffusion literature field considerably, there is still a great amount of material available.

Several bibliographies cover the broad spectrum of diffusion work. Jaumot (22) has prepared a bibliography on diffusion of gases, liquids, and solids in solids over the period 1890-1955. Berard (23) has assembled a bibliography on diffusion in ceramic systems. The proceedings of a symposium held at Gaithersburg, Maryland, in 1967 (24) deals with mass transport in oxides. Also, a quarterly report is published on diffusion data (25).

Among the books which deal with diffusion (i.e., diffusion theory, diffusion mechanisms, mathematics of diffusion, types

of diffusion) are those written by Barrer (26), Jost (27), Shewmon (28), Manning (29), and Crank (30).

Several investigators have studied the diffusion of various transition metals into single crystals of magnesium oxide. Several investigators have used the radioactive tracer technique. Rungis and Mortlock (31) studied radioactive calcium diffusion in magnesium oxide; Harding (32) investigated radioactive barium diffusion in magnesium oxide; and Lindner, and Parfitt (33) studied the self-diffusion of radioactive magnesium in magnesium oxide. Zaplatynsky (34) used a micrographic method of measuring the color penetration for the diffusion of cobalt and nickel in magnesium oxide as did Rigby and Cutler (35) for the interdiffusion of iron in magnesium oxide. Wuensch and Vasilos (36, 37) measured the diffusion of cobalt, zinc, iron, and nickel in magnesium oxide by electron microprobe technique and by X-ray absorption analysis as did Tagai, Iwai, Iseki, and Saho (38) for the diffusion of iron, manganese, and chromium in magnesium oxide. Blank and Pask (39) reported on the diffusion of iron and nickel in magnesium oxide by the electron microprobe technique, and Jones (40) studied manganese diffusion in magnesium oxide by chemical analysis and by the electron microprobe method.

III. THEORY OF NEUTRON ACTIVATION ANALYSIS

It has been found that the properties of emissions (type, energy, and half-life) from radioactive nuclides are characteristic of the nuclides concerned and can thus be used to identify constituent elements in a mixture. Activation Analysis is the name given to the technique by which activated material is produced by irradiation, and the resultant emission spectra is analyzed to determine the identity and quantity of the elements present.

Neutron Activation Analysis (i.e., the activation is produced by neutron irradiation) is an analytical technique that has gained wide acceptance in the last twenty years (41). It has been applied to many different and varied types of materials of interest to the biologist, chemist, metallurgist, and physicist, among others. The technique has been shown to be a very sensitive method for analyzing many different host materials for certain trace elements. The trace-element sensitivity of Neutron Activation Analysis (NAA) as compared to several other analytical methods is shown in Table 1 (41, 42). NAA can be used both as a qualitative and as a quantitative tool for analysis. Whereas many other techniques rely on the chemical properties of an element to determine its presence and concentration, this technique uses the nuclear properties for this purpose.

Table 1. Trace element sensitivity comparisons (μg/ml)

Element	NAA (Oak Ridge LITR reactor)	Copper spark	Graphite direct-current arc	Flame spectro-photometer	Sensitive color reaction	Amperometric titration
Na	.00035	.1	20.	.002		
Mg	.03	.01	0.1	1.	.06	
Al	.0005	.1	0.2	20.	.002	300.
Cl	.0015				.04	10.
Cr	.01	.05	2.	1.	.02	1.
Mn	.00003	.02	0.2	0.1	.001	0.0003
Fe	.45	.5	0.2	2.	.05	2.
Co	.001	.5		10.	.04	0.5
Cu	.00035		0.2	0.1	.03	10.
Zn	.002	2.0	20.	2000.	.016	10.
Ge	.002				.08	
As	.0001	5.0	10.		.1	0.4
Br	.00015					200.
Sr	.03	0.5		0.1		
Pd	.00025	0.5		1.	.1	
Nb	.005	0.2		50.		
Sm	.00003	0.2		100.		
Eu	.0000015	0.02				
Sn	.01		0.2	10.		2.

When most stable isotopes are subjected to neutron irradiations, they undergo one of the following transformations leading to nuclides which are unstable or radioactive:

1) (n, γ)

2) (n, α)

3) (n, p)

4) (n, n)

or 5) (n, 2n)

In addition to slow and fast neutron activation, irradiation by other particles, e.g., protons, deuterons, alpha particles, and photons, can be employed. The choice of activation technique depends on the sample to be analyzed. For example, whereas neutron activation of carbon leads to beta active carbon-14 with a half-life of 5730 years (useless for the conventional gamma analysis ordinarily used in activation analysis), photon activation leads to positron active carbon-11 with a half-life of 20.4 minutes. The 0.511 MeV annihilation radiation with the characteristic 20.4 minute half-life can be used to identify the presence of carbon.

Figure 1 illustrates possible activation reactions where the first particle is the bombarding particle and the second is the particle emitted (43).

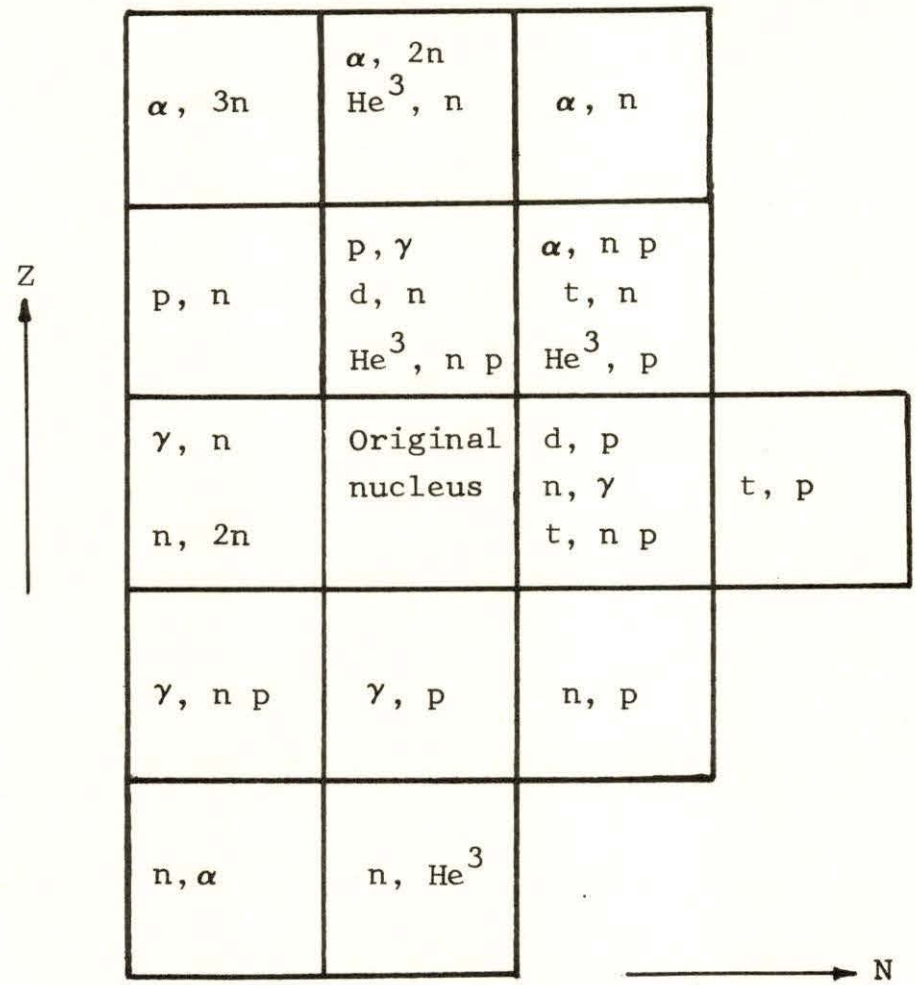

Figure 1. Possible activation reactions

The most likely, hence the most popular reaction, is the (n, γ) reaction which can occur using a thermal neutron (2200 m/sec) reaction. The other four neutron reactions, i.e., (n, α), (n, p), (n, n) and (n, 2n) are caused by epithermal neutrons. The thermal neutron reaction is the most useful for several reasons, among them, the fact that most elements have large thermal absorption cross sections and that very high

thermal flux reactors are available for irradiation purposes. The (n, p) reaction is also popular due to the available source of fast neutrons from 14 MeV neutron generators.

When a nuclide absorbs a thermal neutron, the following reaction can take place:

$$x^{n} + {}_{0}n^{1} \longrightarrow x^{n+1} + \gamma$$

Typical reactions are:

$$^{26}Mg + {}_{0}n^{1} \longrightarrow {}^{27}Mg + \gamma$$

$$^{55}Mn + {}_{0}n^{1} \longrightarrow {}^{56}Mn + \gamma$$

$$^{23}Na + {}_{0}n^{1} \longrightarrow {}^{24}Na + \gamma$$

The important product is the γ-ray or γ-rays that are emitted by the radioactive produce nuclei (e.g., ^{27}Mg). The γ-rays given off have energy characteristics of the nuclides present. Also, the half-life of the radioactive nuclide may be used to help determine the element present in the sample. For instance, there are four different energy γ's that are given off when the stable isotope of Mn, ^{55}Mn, is bombarded by neutrons. These γ-rays have energies of 0.845 MeV (100%), 1.81 MeV (30%), 2.12 MeV (15.3%), and 2.52 MeV (1.2%) (44) where the quantities in parenthesis indicate the percent of decays which yield the given γ-ray. In other words the γ-ray with the energy of 0.845 MeV is given off every time ^{56}Mn disintegrates. The decay scheme of ^{56}Mn is shown in Figure 2 (44).

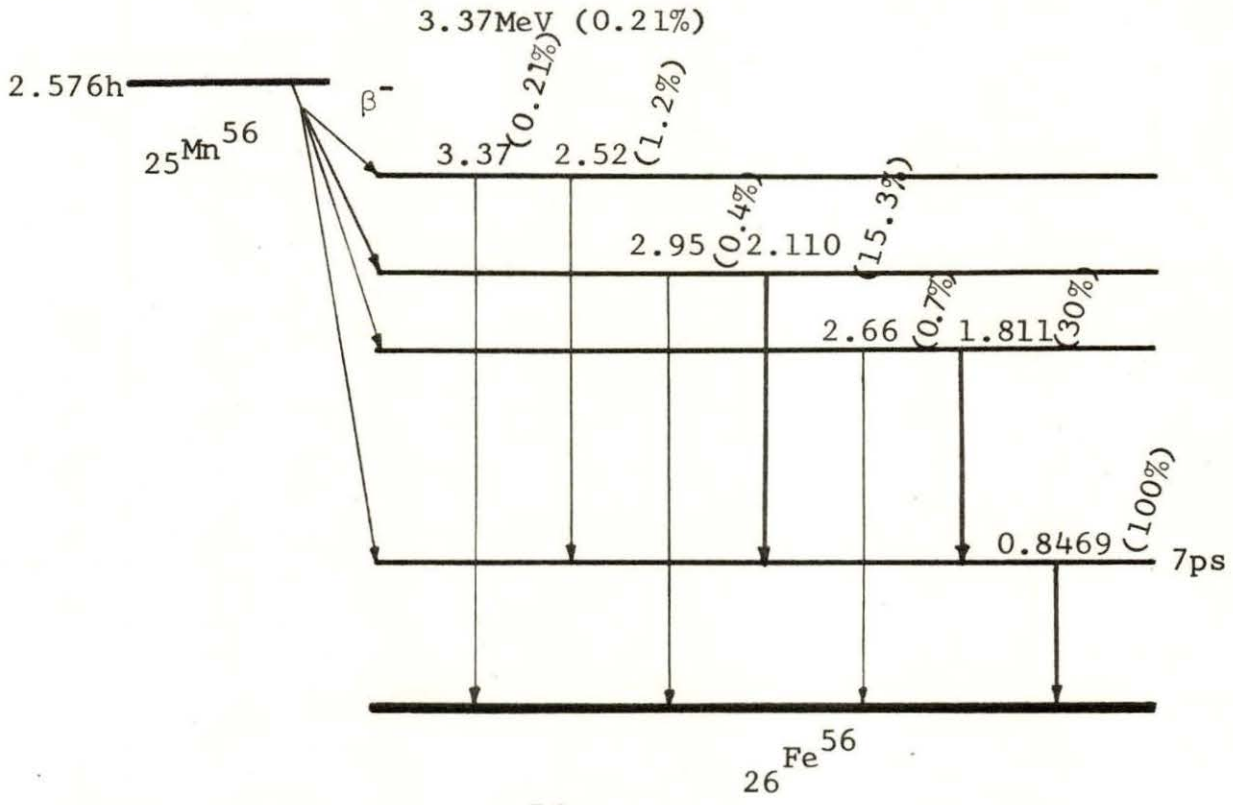

Figure 2. Decay scheme of ^{56}Mn

A. Induced Activity

When a sample is exposed to neutrons several factors go into determining the induced activity. These are: 1) the amounts of the various elements present, 2) the isotopic abundance of the nuclides in question, 3) the cross sections of the nuclides involved, 4) the length of the irradiation, 5) the irradiation flux, and 6) the decay characteristics of the radionuclides produced.

B. Absolute Activity

These factors may be expressed in the following relationship which gives the absolute activity of a single radionuclide produced.

$$D_o = N \sigma \phi (1 - e^{-\lambda t_i}) \qquad (1)$$

where

D_o = Induced absolute activity of the radionuclide at the end of irradiation, dis/sec

N = number of target atoms

σ = activation cross section of target element in cm^2

ϕ = neutron flux neutrons/cm^2 sec

$(1-e^{-\lambda t_i})$ = saturation factor

t_i = irradiation time, sec

λ = the decay constant of the nuclide, sec^{-1}

The number of target atoms present in the sample is given by:

$$N = \frac{\eta_o f w}{A} \qquad (2)$$

where

η_o = Avogadro's number, 6.02×10^{23} atoms/mole

f = fractional isotopic abundance of the target nuclide

w = weight of the element, grams

A = atomic weight of the element, grams

The activity of the radionuclide at any time, t_d, after the end of the irradiation is given by the relationship:

$$D(t) = D_o\, e^{-\lambda t_d} \qquad (3)$$

where

t_d = the time between the end of the irradiation and the time counting begins in sec.

The value for D_o from equation 1 and the value for N from equation 2 can be substituted into equation 3 and the final result is obtained.

$$D(t) = \frac{\eta_o f w}{A}\,(1 - e^{-\lambda t_i})(e^{-\lambda t_d})\sigma\phi \qquad (4)$$

The count rate obtained from a detection system may be converted to absolute activity by using the experimentally determined counting efficiency (including the solid angle correction) of the detector. Thus:

$$\text{Absolute Activity} = \frac{\text{Count rate obtained from detection system}}{\text{Counting efficiency of detection system}} \qquad (5)$$

The counting efficiency of the detection system includes the energy dependent detector efficiency and the counting geometry factor.

C. Interaction of Gamma Rays with Matter

The three principle ways in which gamma rays interact with matter are Compton, photoelectric, and pair production effects (45, 46). These effects are the mechanisms by which the photon energy is converted to electron motion in the NaI(Tl) and Ge (Li) detectors.

1. Photoelectric effect

In the photoelectric interaction all the energy of the photon coming in is absorbed by a bound electron of an atom. The energy of the ejected electron will be equal to the photon energy less the electron binding energy. If the energy of this incoming photon exceeds the binding energy of the K shell, interaction will be almost entirely with the electrons of that shell. As a result of the ejected electron, there is the emission of X-rays or Auger electrons. The X-rays are then generally absorbed by subsequent photoelectric events and the total energy of the incoming photon (less the small fraction involved as binding energy) is absorbed within the detector.

2. Compton process

Along with the photoelectric absorption there is the Compton process, where the incoming photons are scattered by free electrons which receive varying amounts of the initial photon's energy. In the Compton process the energy relationships for the scattered photon and the electron are given by the following equations:

$$E'_{\gamma} = \frac{E_{\gamma}}{1 + E_o(1-\cos\theta)} \qquad (6)$$

$$E_e = E_{\gamma} - \frac{E_{\gamma}}{1 + E_o(1-\cos\theta)} \qquad (7)$$

where

E_γ = incoming gamma ray energy

E_e = scattered electron energy

$E_o = E_\gamma/mc^2$ where mc^2 = .511 MeV

Θ = angle between the direction of the primary and scattered photons

It can be shown from the above equations that there will be a Compton electron energy spectrum from zero energy, where ($\Theta = 0^o$) to a maximum energy at ($\Theta = 180^o$). This maximum energy results in what is called the Compton edge of a gamma ray spectrum.

3. Pair production

If the incoming photon has energy greater than 1.02 MeV which is the rest mass of a positron-electron pair, then pair production is possible. In the pair production process, which must occur in the presence of the Coulomb field of a nucleus, the incoming photon loses 1.02 MeV of energy and a positron-electron pair is produced. The positron thus produced combines with any available electron producing two photons with energies of 0.511 MeV. If one of these annihilation photons escapes from the detector, an "escape" peak appears 0.511 MeV below the actual energy. If both of these photons escape, an "escape" peak at 1.02 MeV below the actual energy is produced.

Therefore the gamma spectrum obtained using these detection systems can be seen to be very complex. A typical gamma

spectrum is shown in Figure 3.

As indicated in the figure, the spectrum consists of Bremsstrahlung, backscatter peak, escape peak or peaks, Compton edge, and full energy peak. The relative magnitude of the various contributions to a particular spectrum depends on the energy of the photons that are being analyzed. In addition, there may be several full energy peaks, as for the ^{38}Cl (gamma spectrum shown in Figure 3). Although the whole spectrum may be used to help identify a particular radionuclide, the full energy peaks are of greatest use.

D. Detection Systems

In this section the photon detection systems that were employed in this work will be described. There are several γ-ray detectors that may be employed (47). The two most common are the Ge(Li) detector and the NaI(Tl) detector.

1. Ge(Li) detector

The incoming γ-ray (photon) is partially or totally absorbed in the sensitive volume producing many charge carriers (electrons and holes). These charge carriers give rise to a current pulse which is amplified and as a signal voltage, enters a multichannel analyzer. This device separates the pulses according to amplitude (or incident photon energy) and records the number of pulses falling in a given amplitude range in appropriate registers or "channels". The complete record in the memory is termed a "profile" or "spectrum". When counting of the sample is complete, the stored counts may be transferred from the

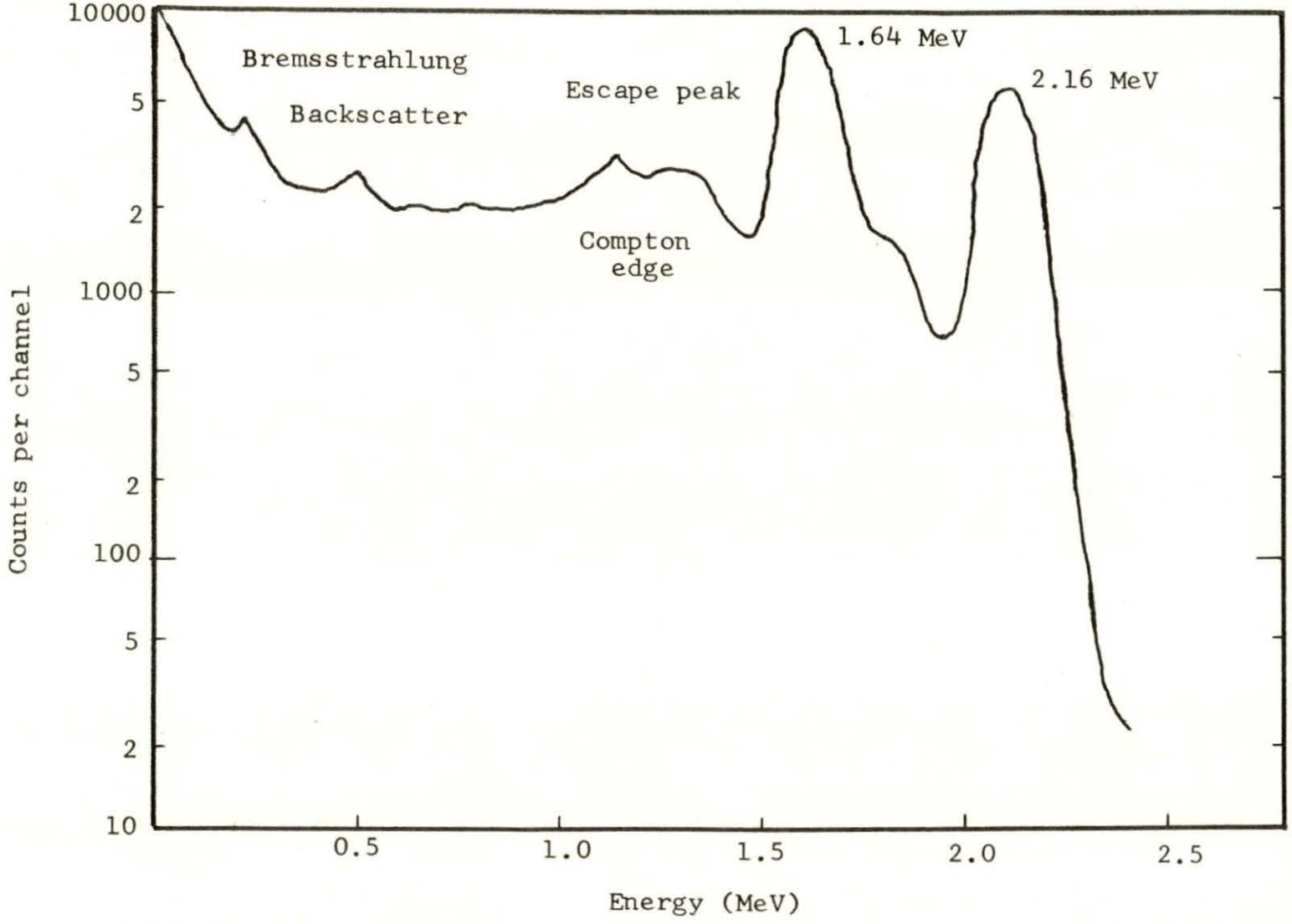

Figure 3. Gamma spectrum of ^{38}Cl

memory by means of an output device, like a teletypewriter, to produce a permanent record (typed page or punched tape). The spectrum accumulated in the memory may, also, be transferred to and stored on magnetic tape and converted to a permanent record at a more convenient time.

2. NaI(Tl detector)

The NaI(Tl) detector system employs a thallium activated NaI single crystal which acts as a scintillator. The γ-ray is absorbed by the crystal which then gives off a light pulse with intensity proportional to the energy of the γ-ray which caused it. A photomultiplier tube then converts the light pulse into a current pulse which is amplified and fed to a multichannel analyzer as in the Ge(Li) system.

The schematic of the detection systems, counting, and data handling equipment is shown in Figure 4.

3. Heath type cave

The counting was carried out in a Heath type cave (45), the inside dimensions of which are 32 in. x 32 in. x 32 in. The cave provides four inch lead walls, the inner surfaces of which are covered first with 0.30 inch thick cadmium sheeting and then with 0.015 inch thick copper sheeting. The lead is used to shield the detector system from outside background radiation; the cadmium and copper act to suppress the lead X-rays produced from photoelectric absorption in the lead shield; the large inside dimensions are required to reduce the

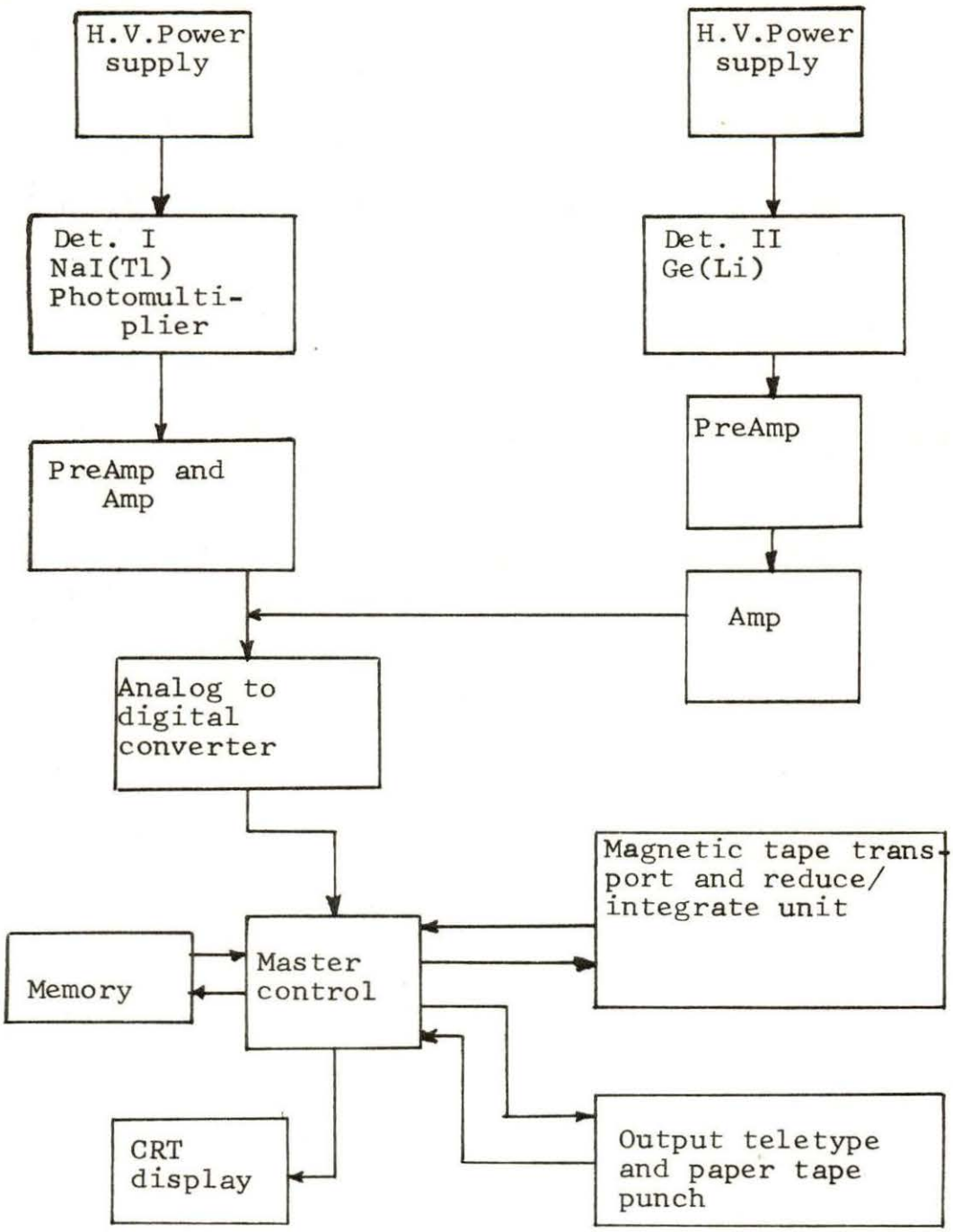

Figure 4. Schematic of detection system

backscatter of the gamma rays from the shield walls. The cave and detection systems are shown in Figures 5, 6 and 7.

E. Counting Time

The length of time that a particular sample is counted depends upon the activity of the sample. Since radioactive decay is a random statistical process, the sample should be counted long enough to give good counting statistics. The uncertainty in a count is given by σ, i.e., the count is represented by $C \pm \sigma$, where σ is the standard deviation, taken to be the square root of the number of counts ($\sigma = \sqrt{C}$).

Therefore, as can be seen, the greater the activity of the sample or the longer the sample is counted, the more certain is the result. Of course, other considerations may require a shorter counting time, e.g., it may be required to count many samples as quickly as possible. In general for this study counting times of 100 seconds were used.

F. Quantitative Analysis

The procedures used in employing neutron activation analysis as a tool in quantitative analysis is described below.

There are two methods that may be used in carrying out a quantitative analysis for a particular element using neutron activation analysis: (7) the absolute method and the comparitor method.

1. Absolute method

The absolute method, which makes use of equation 1, is

Figure 5. Gamma ray spectrometer system

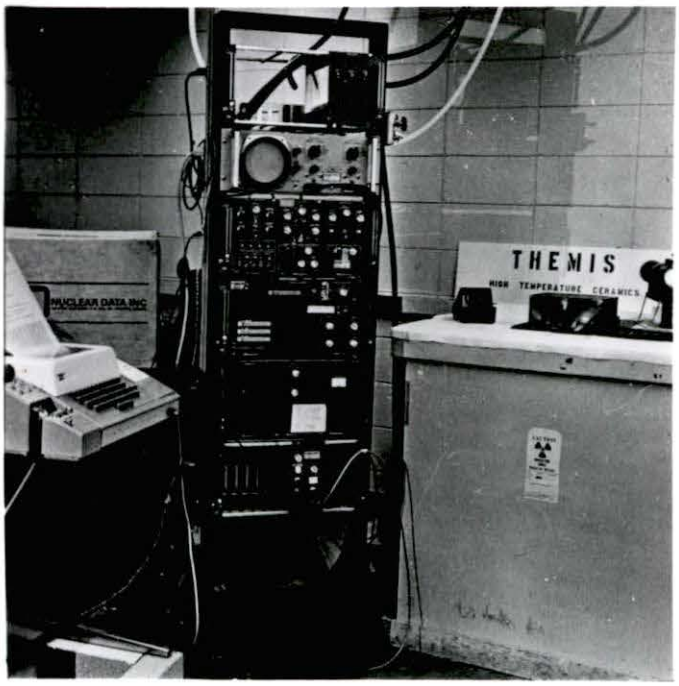
NUCLEAR DATA INC
THEMIS
HIGH TEMPERATURE CERAMICS

Figure 6. Heath type cave, Ge(Li) and NaI(Tl) detectors, and sample holder

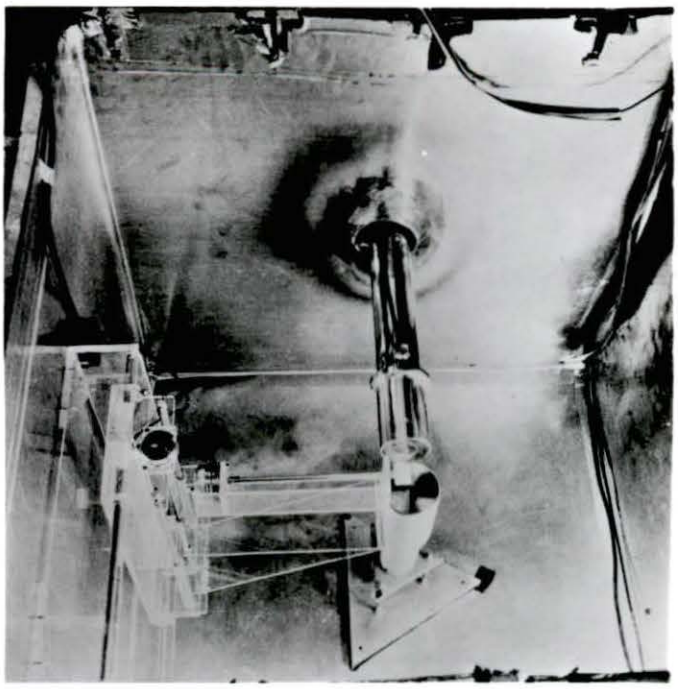

Figure 7. Ge(Li) detector with cryostat and dewar

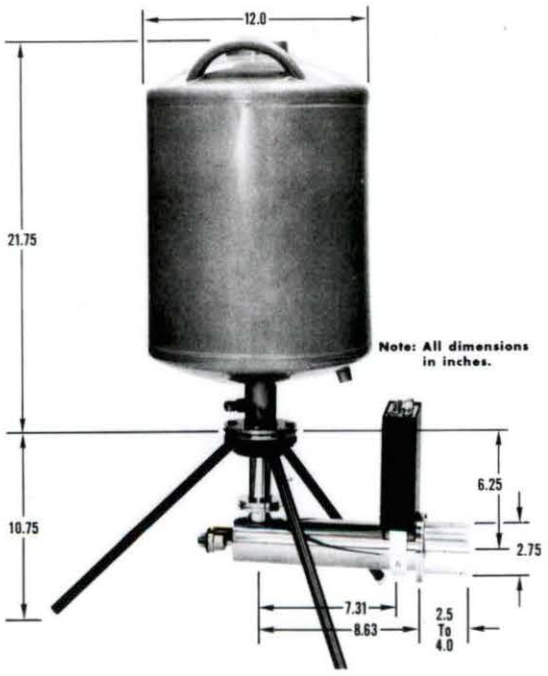
12.0
21.75
10.75
6.25
2.75
7.31
8.63
2.5
To
4.0
Note: All dimensions
in inches.

very seldom used because of the difficulty in obtaining accurate values for the required parameters, viz. the neutron flux, the cross section of the nuclide being studied, the counting efficiency of the detection system, the isotopic abundance, etc.

2. Comparitor method

The comparitor method does not require an accurate knowledge of the neutron flux, the cross-section, the counting efficiency, and the isotopic abundance. In this method, a standard is irradiated at the same time and under the same conditions as the sample to be analyzed. Using the counts accumulated in the full-energy peak and correcting for the difference in the decay times of the sample, or samples, and the standard, the amount of the element in question may be determined. The ratio of the decay corrected counts in the full energy peak of the standard, to its weight is equal to the decay corrected counts, in the full energy peak of the sample, to its weight. This can be expressed by:

$$\frac{X_{std}}{W_{std}} = \frac{X_{element}}{W_{element}} \tag{8}$$

and

$$W_{element} = \frac{X_{element} W_{std}}{X_{std}} \tag{9}$$

where

X_{std} = decay corrected counts or peak area of full energy peak of standard

W_{std} = weight of element in the standard

$X_{element}$ = decay corrected counts or peak area of full energy peak of sample

$W_{element}$ = weight of the element present in the sample being analyzed.

All of the other factors cancel out and thus an accurate knowledge of the parameters required in the absolute method are not required in the comparitor method. It is necessary, however, to know the weight of the standard and to measure the corresponding peak area.

This relationship assumes that the sample and standards are essentially identical and are subjected to the same neutron flux. Because of the possibility of spacial flux variations, the sample and standard must be placed as close together as possible during the irradiation. It is also important to have the concentration of the standard as near to that of the sample as possible. This must be done so that the standard is not so active that it can not be counted at the same time as the samples are counted.

G. Peak Area Determination

There are several techniques used in determining the peak area of the full energy peak (18,45,48). The background contribution is determined by drawing a straight line tangent to the boundaries of the full energy peak as in Figure 8.

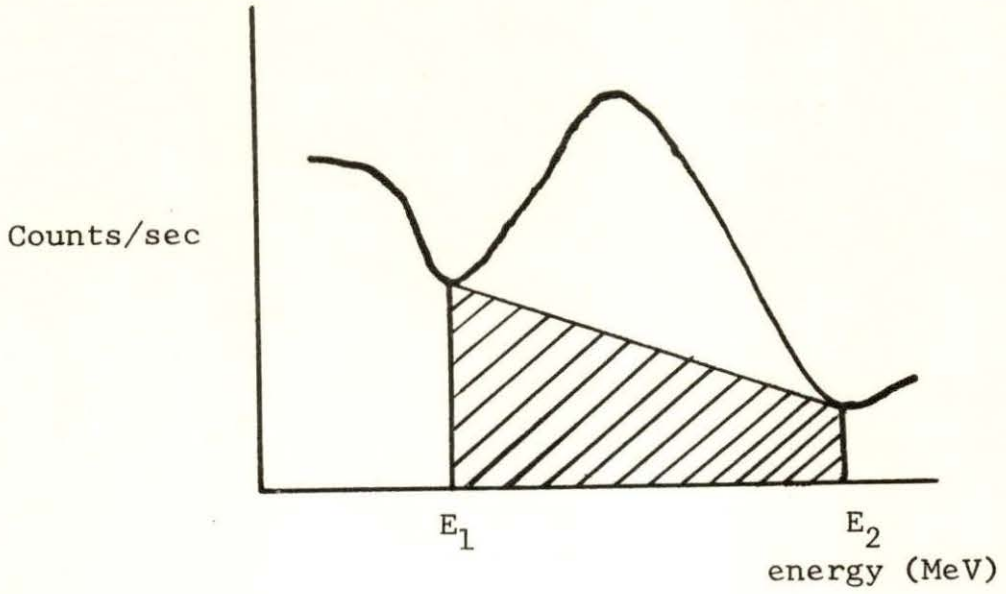

Figure 8. Determination of area of full energy peak by subtraction of background under full-energy peak feet

Any error in locating the baseline results in an error in the area. However, since the unknown and standard have nearly equal peak areas (due to the fact that the standard concentration is made nearly the same as the concentration of the sample) which are treated in the same manner, the errors tend to cancel when the comparison is made.

Peak areas are generally obtained with computer assistance. Since the high resolution capability of the Ge(Li) detector was not required, it was felt to be an advantage to make use of the high detection efficiency of the NaI detector which gives much broader peaks. Therefore, it was decided to add up the counts in the peaks and not use a computer program in determining the peak areas.

IV. THEORY OF DIFFUSION

Since a purely phenomenological approach to diffusion is being taken, it will suffice to develop the equation that is applied in calculating the diffusion coefficient.

Like heat conduction, diffusion is a process attributable to random molecular motion, therefore in 1855 Fick (30) applied the mathematical approach developed earlier by Fourier for heat conduction, and the hypothesis that the rate of transfer of a diffusing substance through unit cross sectional area is proportional to the concentration gradient normal to the section (in Crank (30)). Thus Fick's first law may be written:

$$J = -D \frac{\partial c}{\partial x} \tag{10}$$

where

J = rate of transfer per unit area of section

c = concentration of diffusing substance

x = space coordinate measured normal to the section

D = diffusion coefficient

Fick's first law may be used in deriving the fundamental differential equation of diffusion, Fick's second law, by considering the concentration change with time in an elemental volume. Thus:

$$\frac{\partial c}{\partial t} = - \nabla J \tag{11}$$

where

t = time.

For one-dimensional diffusion, which is a proper restriction for this study, equation 11 reduces to

$$\frac{\partial c}{\partial t} = \frac{\partial}{\partial x}\left(D \frac{\partial c}{\partial x}\right) \tag{12}$$

If D is not constant but is a function of concentration as is the case in this study, then

$$\frac{\partial c}{\partial t} = \frac{\partial D}{\partial x} \frac{\partial c}{\partial x} + D \frac{\partial^2 c}{\partial x^2} \tag{13}$$

The term $\partial D/\partial x$ makes equation 13 nonhomogeneous and a solution difficult.

The solution to equation 13 appropriate for this work is obtained from the Boltzmann-Matano analysis (28) in the following manner.

If the initial conditions can be described in terms of a new variable $z = x/t^{1/2}$, then c is a function of the single variable z and equation 13 can be transformed into an ordinary homogeneous differential equation.

$$\frac{\partial c}{\partial t} = \frac{\partial z}{\partial t} \frac{dc}{dz} = \frac{\partial x t^{-1/2}}{\partial t} \frac{dc}{dz} = \frac{-x}{2t^{3/2}} \frac{dc}{dz} \tag{14}$$

and

$$\frac{\partial c}{\partial x} = \frac{\partial z}{\partial x} \frac{dc}{dz} = \frac{\partial x t^{-1/2}}{\partial x} \frac{dc}{dz} = \frac{1}{t^{1/2}} \frac{dc}{dz} \tag{15}$$

Substituting into equation 12:

$$\frac{-x}{2t^{3/2}} \frac{dc}{dz} = \frac{\partial}{\partial x}\left(\frac{D}{t^{1/2}} \frac{dc}{dz}\right) = \frac{1}{t} \frac{d}{dz}\left(D \frac{dc}{dz}\right) \tag{16}$$

And from $z = x/t^{1/2}$:

$$\frac{-z}{2} \quad \frac{dc}{dz} = \frac{d}{dz}\left(\frac{Ddc}{dz}\right) \tag{17}$$

For the case of the infinite diffusion couple, the following initial conditions may be realized:

$c = C_o$ for $x < 0$, at $t = 0$

$c = 0$ for $x > 0$, at $t = 0$

with the following boundary conditions

$c = 0$, $x = \infty$, all t

$c = C_o$, $x = -\infty$, all t

Eliminating $1/dz$ in equation 17 and integrating between $c = 0$ and $c = C'$ where $0 < C' < C_o$ gives:

$$-\frac{1}{2} \int_{c=0}^{c=C'} z\,dc = \left[\frac{Ddc}{dz}\right]_{c=0}^{c=C'} \tag{18}$$

Substituting $z = x/t^{1/2}$ in equation 18 and using the fact that $dc/dz = 0$ at $c = 0$

$$-\frac{1}{2} \int_{0}^{C'} x\,dc = D(C')t\left(\frac{dc}{dx}\right)_{c=C'} \tag{19}$$

$dc/dx = 0$ at $c = C_o$ therefore:

$$\int_{0}^{C_o} x\,dc = 0 \tag{20}$$

Finally,

$$D(C') = -\frac{1}{2t}\left(\frac{dx}{dc}\right)_{C'} \int_0^{C'} x\,dc \qquad (21)$$

where

D(C') = the interdiffusion coefficient for the system at composition C'.

Equation 21 is called the Boltzmann-Matano solution which is the solution used in this study. The quantities which are required to calculate a value of D in equation 21 are obtained from a plot of C/C_o vs. X. The Matano interface is the plane at which X = 0 in equation 20. An example of this plot is shown in Figure 9. For instance values required to calculate D at $C = 0.3C_o$ are the inverse of the slope and the cross-hatched area shown in Figure 9.

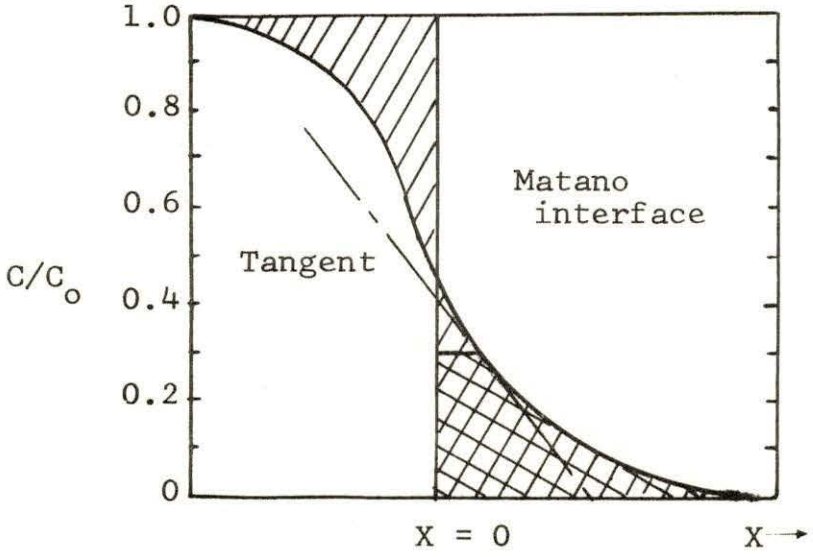

Figure 9. Application of Boltzmann-Matano equation

In many systems the Matano interface is not the original composition discontinuity, but for the system Mn_xO-MgO the Matano interface is assumed to be the original interface for the following reasons:[1] (1) The rigid oxygen lattice structure in magnesium oxide due to the large activation energy of the oxygen, and (2) the impurity ions (manganese) cannot diffuse into the magnesium oxide crystal any faster than magnesium ions move out even though they may have a larger diffusion coefficient, since the oxide does not behave as a semi-conductor. Thus there can be no Kirkendall effect in this system, and therefore, the original interface is indeed the Matano interface.

[1] Jones, John T., Ames, Iowa. Private communication. 1970.

V. EXPERIMENTAL TECHNIQUE

The diffusion measurements carried out on the Mn_xO-MgO system required a) the preparation of the host material (MgO single crystal), b) the fabrication of the diffusant source (a pressed and sintered pellet made from a solid solution of MnO and MgO), c) a diffusion anneal, d) neutron activation of the diffused crystal, e) sectioning, f) determination of diffusant concentrations and g) determination of section thickness.

A. Preparation of Crystals

Most of the MgO single crystals, used in the diffusion studies, were obtained cleaved to a particular size. They were then lapped, using silicon carbide abrasive paper with the apparatus shown in Figures 10 and 11 to produce a rectangular parallelopiped. The crystal was first lapped using 400 grit abrasive paper and finally using 600 grit abrasive paper. The fact that the two crystal faces which defined the diffusion direction were parallel was insured by using the sectioning device (49) described in detail below.

B. Sectioning Device

The main unit of the sectioning device as shown in Figures 12 and 13 is a four-speed phonograph turntable. Above the turntable and parallel to it is a 1/2-inch thick aluminum plate supported by three legs attached to a frame which supports and locates the turntable. In the center of the plate is a hole

Figure 10. Lapping tool, abrasive paper, and MgO crystals

Figure 11. Lapping tool, abrasive paper, and MgO crystals

Figure 12. Sectioning device

Figure 13. Close-up of sectioning device

with a bushing which positions the shaft of the specimen holder perpendicular to the plane of the turntable. This bushing allows free rotation of the specimen holder. The specimen holder consists of a 1/2-inch Jacobs chuck and a length of 1/2-inch diameter drill stock, the ends of which are machined parallel and normal to the axis of rotation and to which the sample is attached by means of a special wax. The sample was mounted on the drill stock using the jig shown in Figure 14. This apparatus insures that the face of the crystal opposite the face, into which diffusion occurs, is held firmly against the end of the drill stock holder while a bond is being established. The drill stock and specimen were placed in the jig as in Figure 14 and the entire assembly heated to 100°C (on a hot plate) to allow the Loc-Wax-20 to melt and, in cooling, to develop a bond between specimen and drill stock. When cool, the drill stock and specimen were removed from the jig and placed in the Jacobs chuck as in Figure 15.

The abrasive paper (1-3/4 inches in diameter) was clamped in the center of the turntable by a ring secured by two nuts running on bolts fastened to the grinding surface bed. Figure 16 shows the sectioning device and Cahn Electro balance in the sectioning hood.

C. Preparation of Solid Solution

The solid solution, which was made up of varying concentrations of MnO-MgO, was prepared in the following manner. For

Figure 14. Jig used in mounting crystal with crystal and drill stock in place

Figure 15. Jacobs chuck containing specimen mounted on drill stock and abrasive paper

Figure 16. Sectioning hood showing sectioning device, Cahn electro-balance, and Mylar tape dispenser


CRAIN

a selected concentration ratio of MnO to MgO, the proper weights of $MnCO_3$ and MgO as dry powders were obtained using an analytical balance. The dry powders were then mixed for five minutes using mortar and pestle and then placed in a jar and, using a tumbling machine, tumbled for one to two hours to insure complete mixing. The mixture was then placed in an Al_2O_3 boat and heated to 1000°C in a gas furnace for two hours to decompose the $MnCO_3$ to MnO. After cooling, the material was reground using a mortar and pestle to 100 mesh screen size. The mixture was then put in a MgO boat and fired in a gas furnace at an appropriate temperature which is very critical (50) as can be seen from the phase diagram for the system MgO-manganese oxide in air (see Figure 17). The temperature must be such that the system is in the (MnMg)O solid solution phase. For instance, for a solid-solution composed of 75 wt. % MnO-25 wt. % MgO, the temperature must be above 1520°C. After firing at the required temperature for 24 hours the solid solution was allowed to cool and then was crushed and mixed in a mortar and pestle. The solid solution was then pressed into pellets using the pellet press and pellet die shown in Figures 18 and 19. The pellets were placed under a pressure of 5000 psig for five minutes. The pellets were next sintered for 12 hours in a gas furnace at a temperature of 100°C above the temperature at which diffusion was to take place, which was usually 1300°C. The sintering operation was required in order to densify the solid solution so that shrinkage would not occur during actual

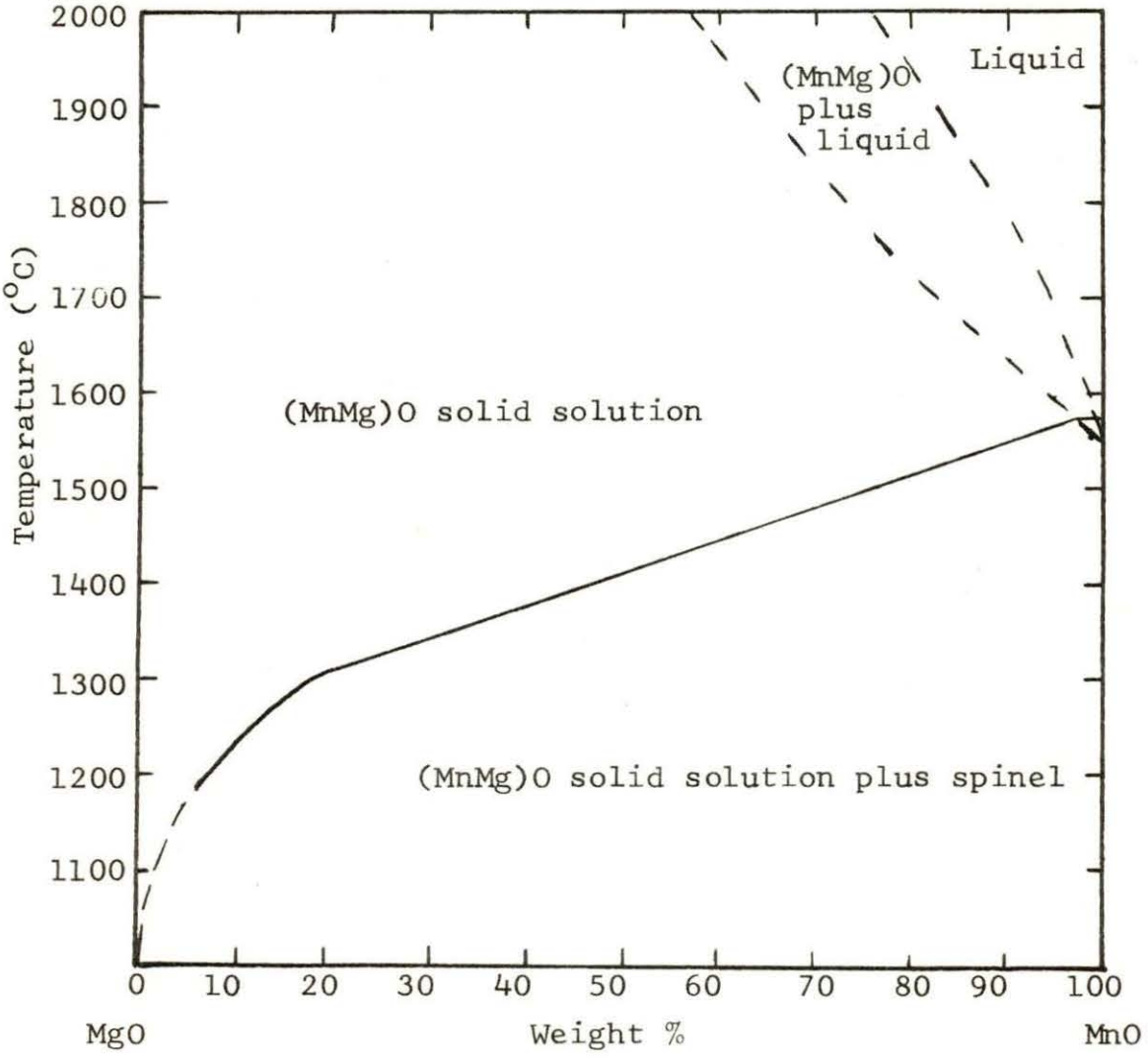

Figure 17. Phase diagram of the system MnO-MgO in air

Figure 18. Pellet press with pellet die

Figure 19. Pellet die and pressed solid solution pellets

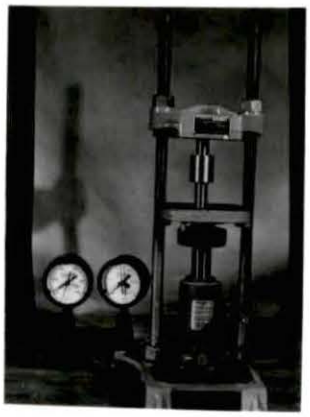

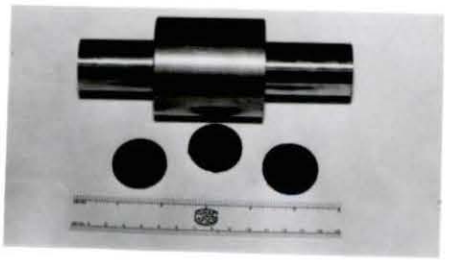

diffusion. (It was found that during the anneal the unsintered pellet would shrink around the crystal and after cooling the crystal was stuck in the pellet.)

After cooling, the face of the pellet to be used for diffusion was polished to insure complete contact between pellet and crystal. The pellet, being round, had to be cut to the dimensions of the crystals in order to make certain that the diffusion boundary conditions were met.

After lapping the MgO crystal and polishing the diffusion face, using 600 grit silicon carbide abrasive and water, the crystal was cleaned. The cleaning process was intended to eliminate surface impurities before the diffusion anneal took place. Cleaning was accomplished by washing with a dilute solution of HNO_3, then distilled water, and finally acetone. The crystal was then allowed to dry in air. This step completed the preparation of the crystal and solid solution pellet for the diffusion anneal.

D. The Diffusion Anneal

Two different furnaces were used for the diffusion anneal. One was a gas furnace (Figure 20), the other an electric furnace (Figure 21).

The crystal was placed on the solid solution pellet and either a platinum wire or platinum sheeting was used to hold the crystal and pellet in contact. The pellet and crystal were then placed in an Al_2O_3 boat.

Figure 20. Gas furnace

Figure 21. Electric furnace

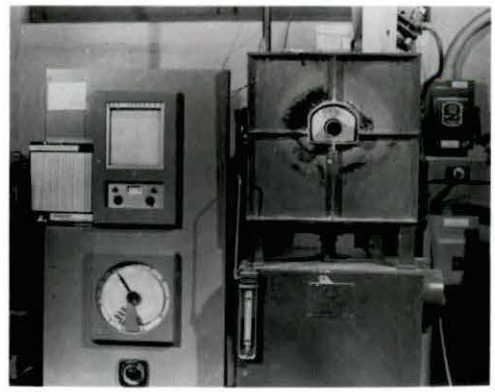

The furnace was raised to the proper temperature, equilibrium was established over a period of 10-14 hours, then the boat and diffusion system were put into the furnace. Care had to be exercised in placing the sample into the furnace so as not to crack the crystal or break the boat. The insertion process was carried out very slowly. The boat and contents were first put into the mouth of the tube of the furnace and left there for five minutes and allowed to equilibrate. Then it was pushed in a short distance and again allowed to equilibrate. This procedure was continued until the center of the furnace had been reached. At that moment the timer for the diffusion anneal was started. The diffusion time and temperature depended upon the depth of diffusion desired. The temperature range for the purpose of this study varied from 1300°C to 1540°C. The length of annealing time varied from 7 to 17 hours. The preliminary anneals were carried out at the various temperatures and annealing times, but the final experiments were carried out at 1300°C for 16 to 60 hours.

When the desired diffusion time was reached, the sample was removed from the furnace in a similar manner to the way in which it was introduced.

When the sample had cooled, it was taken off the pellet and was then ready for pre-irradiation preparation.

E. Preparation of Sample Before Irradiation

1. Removing unwanted surface diffusion

It was found that the way in which the diffusion anneal was performed permitted diffusion to take place into all faces of the MgO crystal. Two possible reasons for this effect are: one, surface diffusion, i.e., the Mn ions move around the edge of the crystal and then diffuse into the side faces, and, two, some of the solid solution vaporizes, condenses onto the exposed surface of the crystal and then diffuses into the side faces and top. Diffusion taking place from the top of the crystal has no effect on the study of diffusion into the desired face; but, the diffusion of the Mn ions into the side faces definitely interferes with measurements. Therefore, it was imperative that the material which diffused into the sides of the crystal be removed. To determine the diffusion penetration of the sides, an electron microprobe analysis was carried out indicating a penetration of the order of 5 microns. Based on this information the four side faces were lapped as before, using the special lapping tool with 400 and 600 grit silicon carbide abrasive paper, to the proper depth to remove this unwanted diffusion contribution. Finally the dimensions of the crystal were determined using a micrometer. These dimensions are required to determine the diffusion surface area of the crystal.

2. Cleaning the crystal

The crystal was then cleaned to remove surface contamination which might activate and interfere with the determination of the diffusion coefficient. A second reason for trying to eliminate surface contamination is to keep the overall activity of the sample as low as possible so that the sectioning can be done with minimum delay. The cleaning procedure involves the following steps. First the crystal was washed in a solution of dilute HNO_3. The crystal was placed in a beaker of dilute HNO_3 solution and stirred magnetically for five minutes. The crystal was then washed in distilled water for five minutes using the same procedure, rinsed with acetone, and allowed to dry by evaporation. The sample was then weighed using an analytical balance. Following sectioning, the remaining crystal was again weighed permitting a determination of the total amount of material removed.

After the crystal was cleaned, care was taken not to again contaminate the crystal. For example, contact between crystal and the hands could contaminate the sample with NaCl. ^{24}Na has a half-life of 15.0 hours and γ-energies of 1.368 MeV, 2.754 MeV, 3.85 MeV and 4.23 MeV (44). ^{38}Cl has a half-life of 37.3 minutes with γ-energies of 1.60 MeV, 2.17 MeV, and 3.76 MeV (44). These energies will not interfere with the energies of interest for the Mn, but they would add to background of the γ-spectrum and would also increase the activity of the sample. Therefore, the sample was handled with tweezers that had

been cleaned in much the same way as had the crystal. That is, they were washed with dilute HNO_3, then with distilled water, rinsed with acetone, and dried.

3. Preparation of manganese standard

Since the comparitor method was used in this study, a manganese standard had to be prepared and irradiated at the same time and under the same conditions as the diffusion sample. The standard was prepared in the following manner. It was desired to have the amount of the manganese in the standard correspond to the average amount of the manganese in the sections. After an experimental determination of the most suitable concentration a solution of manganese standard was prepared by dissolving an appropriate weight of manganese dioxide in 200 milliliters of distilled water with the assistance of two milliliters of hydrogen perioxide and approximately 10 milliliters of nitric acid. Then enough distilled water was added to produce 1000 milliliters of solution in a volumetric flask. Two concentrations were made, one yielded a concentration of 8×10^{-5} grams/milliliter and the other a concentration of 1×10^{-4} grams/milliliter. The standards were made up using one milliliter volumetric pipettes. The containers used for the standards were two milliliter polyethylene vials. After pipetting the standard into the precleaned polyvial, the liquid was evaporated to dryness in an oven at $70^{\circ}C$, a process which generally took 10-12 hours. The drying process

could leave manganese residue in varying amounts on the sides as well as the bottom of the polyvial which would explain the experimentally observed variation in count rate from supposedly identical standards. To test this hypothesis, tests were conducted on manganese standards left as solutions. The results of this work is given in the discussion section.

Similarly, the crystal was put into a separate precleaned polyvial and in order to insure that the cleaned and loaded polyvials would receive no further contamination, they were enclosed in sealed plastic envelopes (fingers cut from plastic gloves and heat sealed shut). Thus, the protected samples could then be handled freely without fear of contaminating the crystal, the standard, or the polyvial in which they were contained. After completing the pre-irradiation preparation of the crystal and standard, a radiation request form was completed (see Figure 22).

F. Irradiation Facility

1. Reactor description

The neutron irradiations were provided by the research reactor operated by Ames Lab of the U.S.A.E.C. The Ames Lab Research Reactor (A.L.R.R.) is a 5 MW tank-type reactor which is cooled and moderated with heavy water and fueled with 93% enriched ^{235}U.

Figure 22. Ames Lab research reactor radiation request form

ALRR IRRADIATION REQUEST

NAME _____ DATE _____

GROUP LEADER _____ REACTOR USAGE NO. _____

CHEMICAL DESCRIPTION _____

_____

AMOUNT AND PHYSICAL DESCRIPTION OF MATERIAL _____

_____

DESCRIPTION OF SAMPLE CONTAINER _____

_____

INTEGRATED FLUX DESIRED (NVT) _____ ACTIVITY DESIRED (μc, mc, c) _____

SPECIAL INSTRUCTIONS _____

_____

The undersigned has inspected the above sample and has determined that the description is correct. _____

Signature of Requestor

TO BE COMPLETED BY REACTOR DIVISION

SAMPLE NUMBER _____

SAMPLE RECEIVED BY _____

SPECIAL INSTRUCTIONS TO BE COMPLETED BY REACTOR OPERATIONS SUPERVISOR

IRRADIATION LOCATION _____

EXPOSURE TIME _____

REMARKS _____

_____

APPROVED FOR IRRADIATION BY _____

2. Experimental irradiation facilities

Preliminary irradiations were carried out in the R-3 and TV-1 experimental irradiation facilities of the A.L.R.R. R-3 provides a pneumatic tube ("rabbit tube") access to a high flux region immediately below the reactor core. The samples placed in capsules ("rabbits") are inserted into and removed from the reactor rapidly by a pneumatic transfer system. The TV-1 facility provides access to the thermal column of the reactor. The thermal column, as its name implies, produces slow (thermal) neutrons. Since the reactions of interest in this study are produced by thermal neutrons, the TV-1 thermal facility was used for the irradiations required. The neutron energy spectrum in TV-1 is characterized by a cadmium ratio of approximately 1000 as compared to a cadmium ratio of approximately 20 found in R-3. The cadmium ratio is given by:

$$R_{Cd} = \frac{\text{Thermal activation of a foil}}{\text{Fast activation of a foil}} + 1 \qquad (22)$$

Therefore, when a thermal flux, with a very small fast neutron component, is required (as was the case for this study) the cadmium ratio should be large.

Whereas the R-3 facility provides a high thermal flux, it also had the disadvantage of a relatively high fast neutron component, i.e., it has a relatively small cadmium ratio. The TV-1 facility, in which most "diffusion" irradiations were performed, being located in the thermal column, thus provides a very low fast flux contribution and thus very few fast neutron

reactions take place.

The samples and standards were loaded into "rabbit" capsules by reactor personnel for R-3 irradiations. For TV-1 irradiations the samples were scotch taped to the bottom of a sample holder and lowered into the thermal column from the top of the reactor. As noted before, sample and standard are irradiated together and are placed close together to permit exposure to the same neutron flux. Actually, two standards were used in each experiment as a check on the accuracy of standard preparation.

G. Irradiation

Since it was necessary to section the crystal while it was radioactive, it was very important to make certain that the radiation dose from the sample was within acceptable limits during the working period. Calculations were carried out using equation 4 on page 12, for both magnesium and manganese. Initially a crystal weight of 300 milligrams was assumed and since the amount of manganese that would diffuse into the MgO crystal was not yet known, an appropriate concentration had to be assumed. It was determined that a 45 minute irradiation in TV-1 would give a reasonable activity for counting purposes after a two hour delay, required for transportation and sectioning after the end of the irradiation. In addition the dose received while sectioning the crystal appeared to be acceptable. Preliminary experiments demonstrated that the 45 minute irradi-

ation was appropriate for the sample size chosen. The 9.5 minute magnesium-27 activity had decayed through two or three half-lives by the time the irradiated sample was received in the sectioning laboratory and had dropped to a relatively low level by the time counting was possible.

Arrangements were made for reactor personnel to start the sample irradiations so that they would be available for sectioning at a convenient time. Health Physics personnel transferred the radioactive samples from the reactor to the laboratory in which the sectioning was carried out.

H. Sectioning

The procedures used in sectioning samples and the preliminary investigations leading up to these procedures are described below.

Although a number of sectioning techniques have been described, it seemed both convenient and appropriate to use available grinding procedures already described.

Considerable preliminary tests were carried out before the actual experiments were performed. Among the questions to be answered by the preliminary work were:

1) What is the most suitable grit size for the silicon carbide abrasive paper to be used in grinding the MgO crystal?
2) How long would it take to grind off the desired thickness of crystal from the sample?

3) How long would it take to carry out the complete sectioning of all of the required sections?

It was also necessary to practice the technique to be used, since the radioactive sample used in the actual experimental work should be handled as little as possible. Since the weight of a MgO section is given by the weight gained by the grinding paper, it was very important that experience be gained in handling the balance used to weigh the abrasive paper before and after sectioning. Since the weight of each section was very small any error in weighing the abrasive paper would cause a large error in the final diffusion coefficient determination. The balance used for this study was a Cahn-Electro balance.

During the actual performance of the sectioning it was necessary to wear rubber gloves to prevent radioactive contamination of the hands. The sample activities at the time sectioning was performed varied from 50 to 200 mrad/hr. depending upon the crystal size, the amount of manganese which was allowed to diffuse into the crystal, and the time which had elapsed between the end of irradiation and the time at which the sectioning was begun.

Upon receipt of the irradiated crystal and the two standards in the sectioning laboratory, the crystal was removed from the polyvial and mounted on the drill stock (or sample holder). The crystal was centered on the end of the drill stock, making certain that the crystal face in which diffusion

had occurred was up, and the combination was placed in the jig, Figure 14. The top of the jig was screwed down making certain that proper contact between the crystal and the end of the drill stock was established. The entire assembly was then heated to 100°C using a hot plate. Small pieces of Loc-Wax-20 were placed around the junction between the crystal and drill stock where they melted. Upon cooling, a Loc-Wax-20 bond was established between the pair. The drill stock with the attached crystal was removed from the jig and placed in the jaws of the Jacobs chuck. The grinding procedure used to section the crystal could now be started. The abrasive paper was pre-cut to the proper size about 24 hours before needed to permit the establishment of moisture equilibrium by the time it was needed.

The abrasive paper was weighed before sectioning and again after sectioning. The difference in weight between the two measurements was the weight of the section removed from the crystal. The crystal was generally ground until a desired section thickness of from 5 to 8 microns was obtained.

After the "section" (abrasive paper plus the portion of the crystal taken off) was taken off and weighed, mylar tape was put over the powder loaded abrasive paper to prevent loss of powder. This precaution made certain that none of the powder on the paper was lost, thus reducing the chances of error in the determination of the amount of crystal taken off in each section, and, equally important, it also made certain

that radioactive debris did not contaminate the area.

From preliminary experiments, it was found that the diffused manganese was contained in the first 20 to 25 sections. Thus, under the conditions which prevailed during the diffusion anneal, manganese penetrated the MgO crystal a distance of about 200 microns. Obviously, there was no point in sectioning beyond this distance. During the actual sectioning of a crystal it was possible to determine that no further sectioning was necessary by observing when the "Cutie Pie" detector measured activity dropped from 30 mrad/hr. for a section to 1 mrad/hr. for the following section.

After sectioning was completed, Health Physics personnel transferred the radioactive sections to the counting laboratory.

I. Counting the Sections

The techniques and methods used to determine the concentration of manganese in each crystal section are described below.

Much experimental work was performed to determine the best way in which to count the sections and standards. There were two types of counting detectors available, a thallium activated NaI scintillation type detector and a lithium-drifted germanium detector.

The decision was made to use the NaI(Tl) detector since the resulting broad peak permitted a more precise area determination. The spectra obtained with the Ge(Li) detector in-

dicated that there would be no interference with the manganese lines from the other peaks after the 9.5 minute magnesium-27 had decayed appreciably.

Since the counting geometry, that is, the placement of the sample with respect to the detector, is assumed to be equal for the two samples when using the comparitor method of analysis, it is necessary to make certain that the samples and standards occupy the same volume in space when being counted. When the NaI(Tl) detector was used there were no problems encountered since it was possible to place each section and the standard in turn on a chosen point on the horizontally positioned beryllium metal absorber which covers the end cap over the crystal face.

When the Ge(Li) detector was used, a positioning problem arose, since, as shown in Figure 6, the Ge(Li) detector comes into the Heath type cave from the side, whereas the NaI(Tl) detector is vertically positioned. For this case, positioning uniformity was provided by the sample holder and sample holder rack shown in Figure 23. Each section was placed in a holder which was allowed to slide down the sample holder rack to a fixed point close to the detector face. The sample holder for the manganese standards is shown in Figure 24.

J. Data Analysis

Upon completion of the counting, the data were analyzed to yield the interdiffusion coefficients for the Mn_xO-MgO systems.

Figure 23. Sample holders and sample holder rack for sections

Figure 24. Sample holder for standards in polyvial

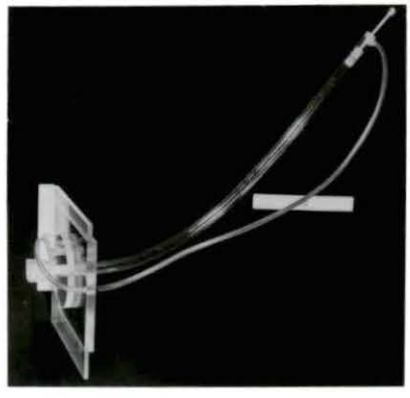

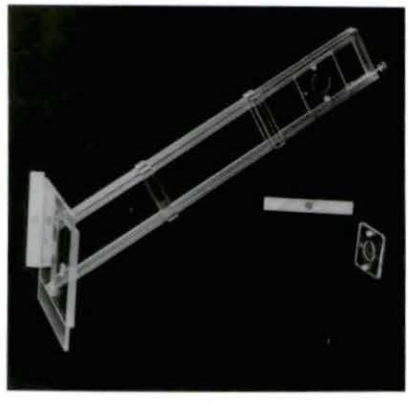

The methods applied in arriving at the desired results from the γ-ray spectra are described in detail below.

1. Selection of full-energy peak

All three of the ^{56}Mn full-energy gamma peaks may be used in determining the amount of manganese present in a given section removed from the crystal. A typical γ-ray spectrum of a section using a Ge(Li) detector is shown in Figure 25. A typical γ-ray spectrum of a section using a NaI(Tl) detector is shown in Figure 26. As can be seen, only the three ^{56}Mn peaks corresponding to photon energies of 0.845 MeV, 1.810 MeV, and 2.120 MeV are present. The peaks of 0.845 MeV and 1.810 MeV were used in the determination of the manganese concentration in each section. The peak at 2.120 MeV was not used due to its low relative intensity as compared to the other two peaks present. The only possibility of interference to either of these two peaks could be from the ^{27}Mg full energy peak of 842 KeV. There should be very little or no contribution to the peak area from the ^{27}Mg since the sections were counted at least two hours, i.e., 12.5 ^{27}Mg half-lives after the end of the irradiation (for the Mn concentrations considered here).

The following steps are required in determining the interdiffusion coefficient for the system Mn_xO-MgO:

1) Find the weight of manganese in each section.

2) Find the weight percent of MnO in each section.

3) Find the volume of each section.

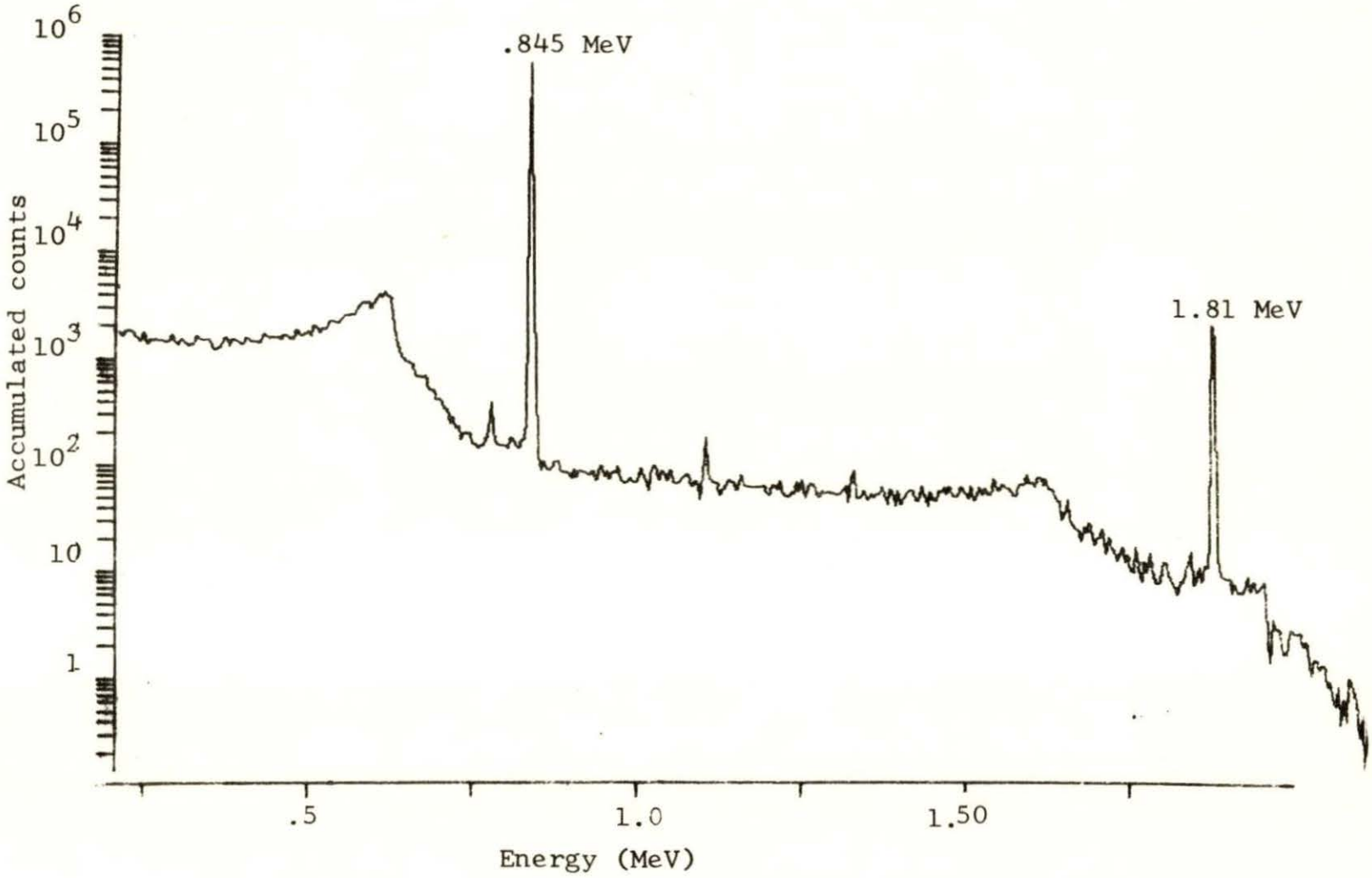

Figure 25. Typical gamma ray spectrum of a section using Ge(Li) detector

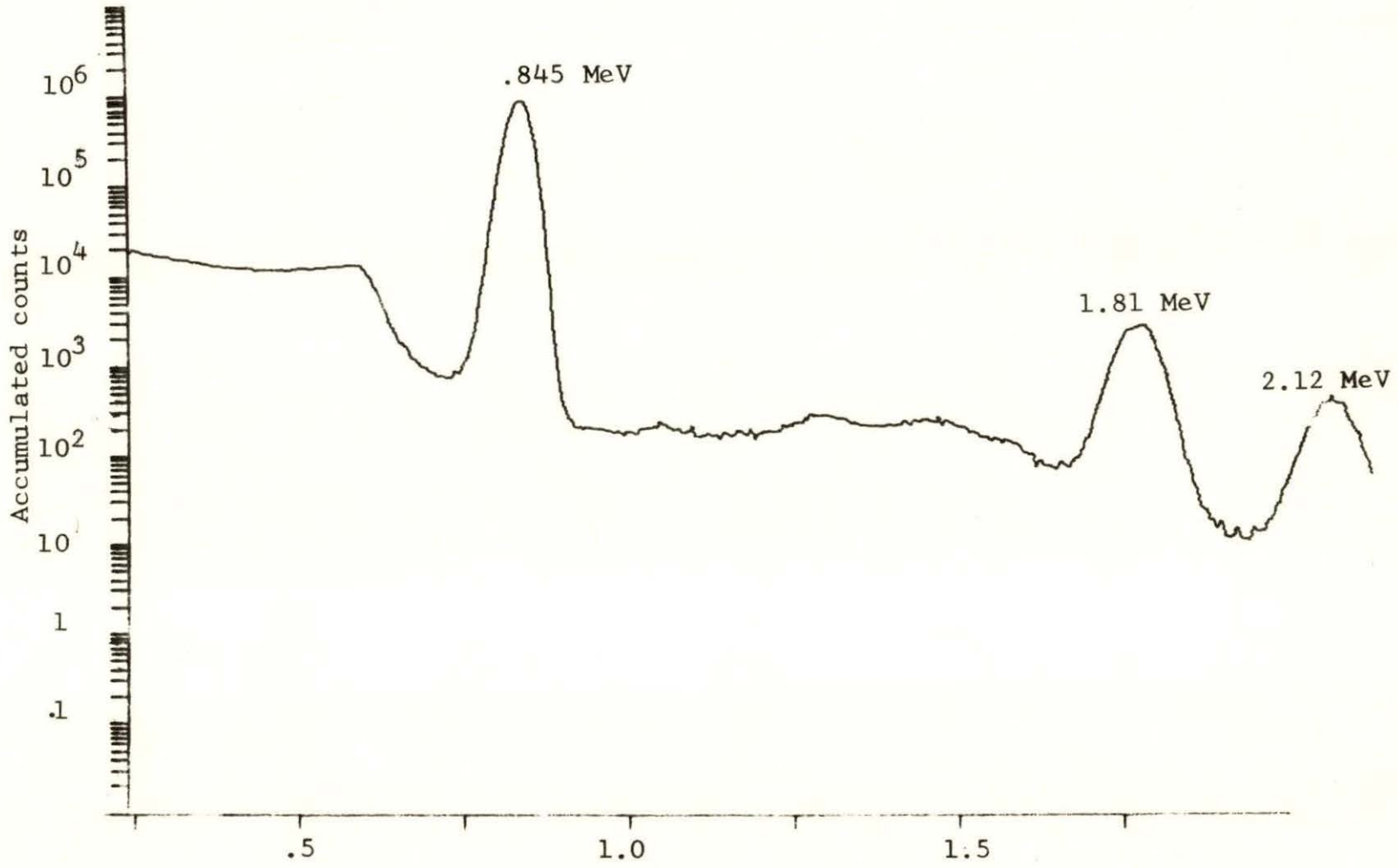

Figure 26. Typical gamma ray spectrum of a section using NaI(Tl) detector

4) Find the thickness of each section.

5) Plot the ratio of the weight percent MnO in each section to the initial weight percent MnO in the solid solution vs. distance into crystal.

6) Apply Boltzmann-Matano equation (equation 21) to the plot in (5) above.

These steps are given in detail below.

2. Determination of weight of manganese

The first step was to determine the amount of manganese in each section. The weight of manganese present in a section is given by the following equation:

$$\text{wt.}_{\text{Mn in section}} = \text{wt.}_{\text{Mn STD}} \frac{\text{P.A.}_{(o)}\text{Mn (1810 KeV) section}}{\text{P.A.}_{(o)}\text{Mn (1810 KeV) STD}} \tag{23}$$

where the peak areas for the sections and the standards were corrected for their different decay times. Thus,

$$\text{P.A.}_{(o)} = \text{P.A. (t)}\ e^{\frac{.693}{t_{1/2}}t} \tag{24}$$

where

P.A.(t) = peak area of full energy peak for ^{56}Mn at time (t) when section was counted.

$\text{P.A.}_{(o)}$ = peak area of full energy peak for ^{56}Mn at the end of irradiation.

$t_{1/2}$ = half-life of Mn, 2.58 hours.

t = decay time or time after the end of irradiation in hours.

After determining the weight of the manganese that diffused into the sections, the amount of oxygen present in each section associated with the manganese was found in the following manner:

$$\text{wt. oxygen in each section corresponding to the Mn} = \text{wt. manganese}\left[\frac{\text{At. wt. oxygen}}{\text{At. wt. manganese}}\right] \quad (25)$$

Therefore:

$$\text{wt. of MnO in each section} = \text{wt. manganese}\left[1+\left(\frac{\text{At.wt.oxygen}}{\text{At.wt.manganese}}\right)\right] \quad (26)$$

Therefore:

$$\text{wt. of MnO in each section} = 1.292\ (\text{wt. manganese}) \quad (27)$$

The weight of MgO in each section can be determined from the total weight of the section and the total weight of MnO calculated using equation 27. Thus:

$$\text{wt. MgO in section} = \text{Total wt. section} - \text{wt. MnO in section} \quad (28)$$

In each unit cell of a MgO single crystal, there are four molecules of MgO. From an article by Jones and Cutler (51) it was determined that, at the concentration of the manganese present in the sections, the small fraction of Mn^{+3} ions diffusing into the MgO crystal would have very little effect on

the number of cations in a unit cell. (A large fraction of Mn^{+3} ions would require the existence of a large number of vacancies to preserve neutrality, i.e., for every two Mn^{+3} ions diffusing into the MgO crystal, one vacancy would develop). Since this posed no problem it was assumed that the number of cations in the unit cell remained constant at four (Mn+Mg) and that there were also four oxygen ions at all times. Therefore in each unit cell of the crystal after diffusion there were still four molecules (MnO and MgO).

From the values obtained using equations 27 and 28 the total number of molecules of MgO and MnO can be obtained using the equation below.

Total number of molecules in the section =

$$\text{wt. MnO in section} \quad \frac{\eta_o}{\text{M. wt. MnO}} + \text{wt. MgO in section} \quad \frac{\eta_o}{\text{M. wt. MgO}} \tag{29}$$

where:

η_o = Avagadro's number, 6.02×10^{23} molecules/gm mole

M. wt. MnO = molecular weight MnO, 70.94 grams/mole

M. wt. MgO - molecular weight MgO, 40.3 grams/mole

Therefore, for each section:

$$\text{Total number of molecules} = 8.5 \times 10^{21} \times \text{wt. MnO} + 14.95 \times 10^{21} \times \text{wt. MgO.} \tag{30}$$

Since there are four molecules per unit cell, then

$$\text{total number unit cells per section} = \frac{\text{total number of molecules (MnO MgO)}}{4} \qquad (31)$$

3. Volume of each section

From the total number of unit cells per section and the lattice parameter of each unit cell, the section volume can be obtained. The lattice parameter for the MnO-MgO system has been found to vary almost linearly with composition from 4.200Å for pure MgO to 4.435Å for pure MnO (52). A plot of the lattice parameter of the MnO-MgO system vs. the wt. % MnO is shown in Figure 27. From this plot, the lattice parameter for any concentration can be obtained. The lattice structure of the MgO unit cell is cubic and it is assumed that when manganese diffuses into the unit cell as the magnesium diffuses out the structure of each unit cell remains cubic. Therefore, the volume of a unit cell is the cube of the lattice parameter, thus the section volume is given by:

$$\text{Volume section} = \text{number unit cells per section} \times [\text{lattice parameter unit cell}]^3 \qquad (32)$$

4. Thickness of each section

Using the measured cross sectional area of the original crystal, the thickness of a section is given by:

$$\text{Thickness section} = \frac{\text{Volume section}}{\text{Cross-sectional area crystal}} \qquad (33)$$

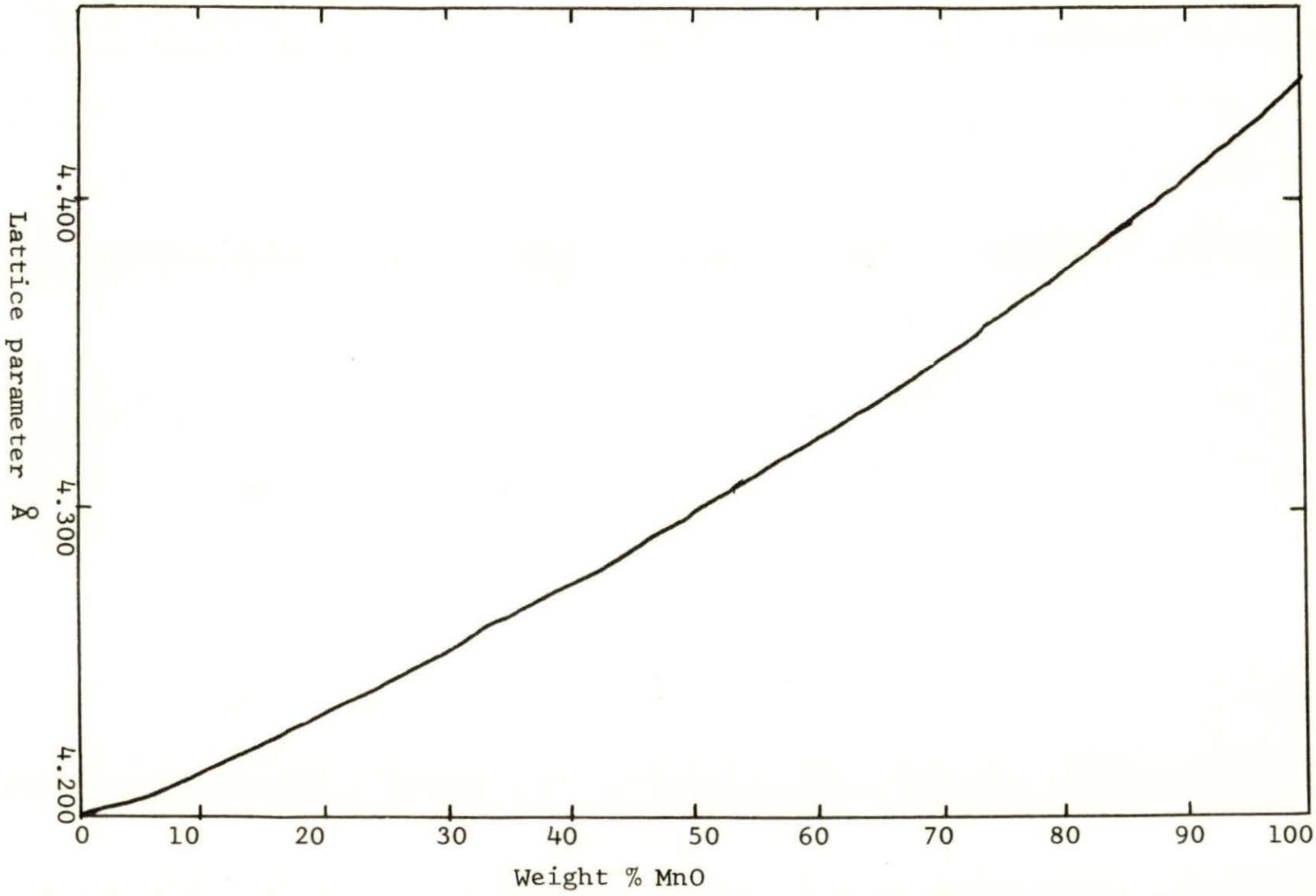

Figure 27. Plot of lattice parameter vs. MnO concentration for the system MnO-MgO

The weight percent of MnO in a section (needed for the determination of the lattice parameter from the plot in Figure 27 is given by:

$$\text{wt. percent MnO in section} = \frac{\text{wt. MnO in section}}{\text{total wt. section}} \times 100\% \quad (34)$$

The mole percent (needed for the interdiffusion coefficient calculation) is found using the following equation:

$$\text{Mole percent MnO per section} = \frac{\text{moles MnO per section} \times 100\%}{\text{moles MnO/section} + \text{moles MgO/section}} \quad (35)$$

5. Interdiffusion coefficient

The interdiffusion coefficient is obtained from a plot of the mole percent MnO vs. the distance into the crystal or from a plot of the ratio of the concentration of MnO in the section to the concentration of MnO in the solid solution vs. the distance into the crystal using the Boltzmann-Matano equation (equation 21).

VI. RESULTS

Experiments 1 through 8 were regarded as preliminary in that they indicated necessary changes in the experimental procedures.

The mole % MnO vs. distance profiles for runs #8, 9, 11, and 12 are shown in Figures 28, 29, 30, and 31. The temperature and length of the diffusion anneal, and solid solution composition are given on the profiles.

From these profiles the interdiffusion coefficients were obtained for runs #9, 11, and 12 using the Boltzmann-Matano equation. These interdiffusion coefficients are plotted vs. mole % MnO in Figure 32.

All of the diffusion anneals were fired in air.

The data for runs #7, 8, 9, 10, 11 and 12 are given in Appendix A.

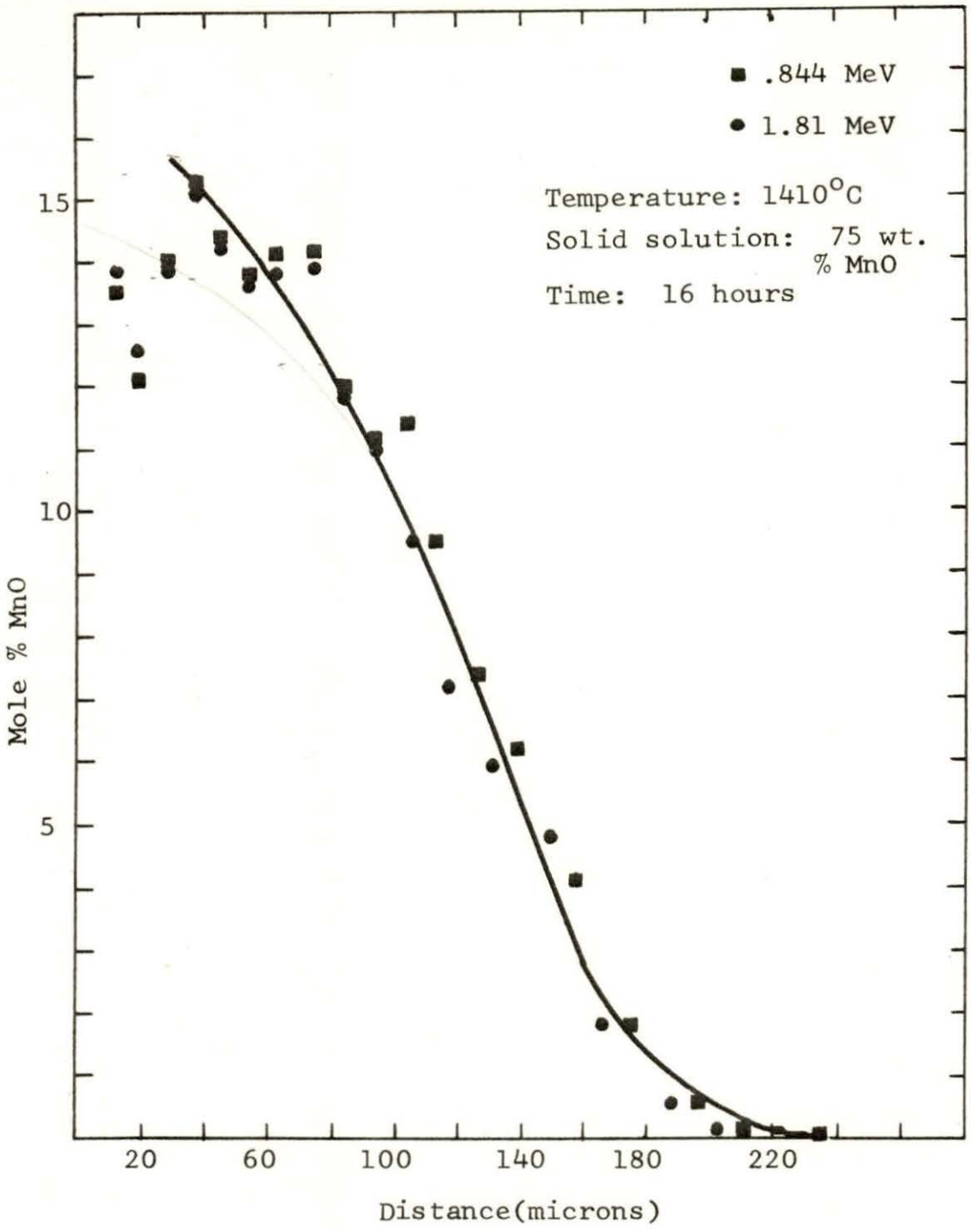

Figure 28. Concentration profile of MnO in single crystal MgO for run #8

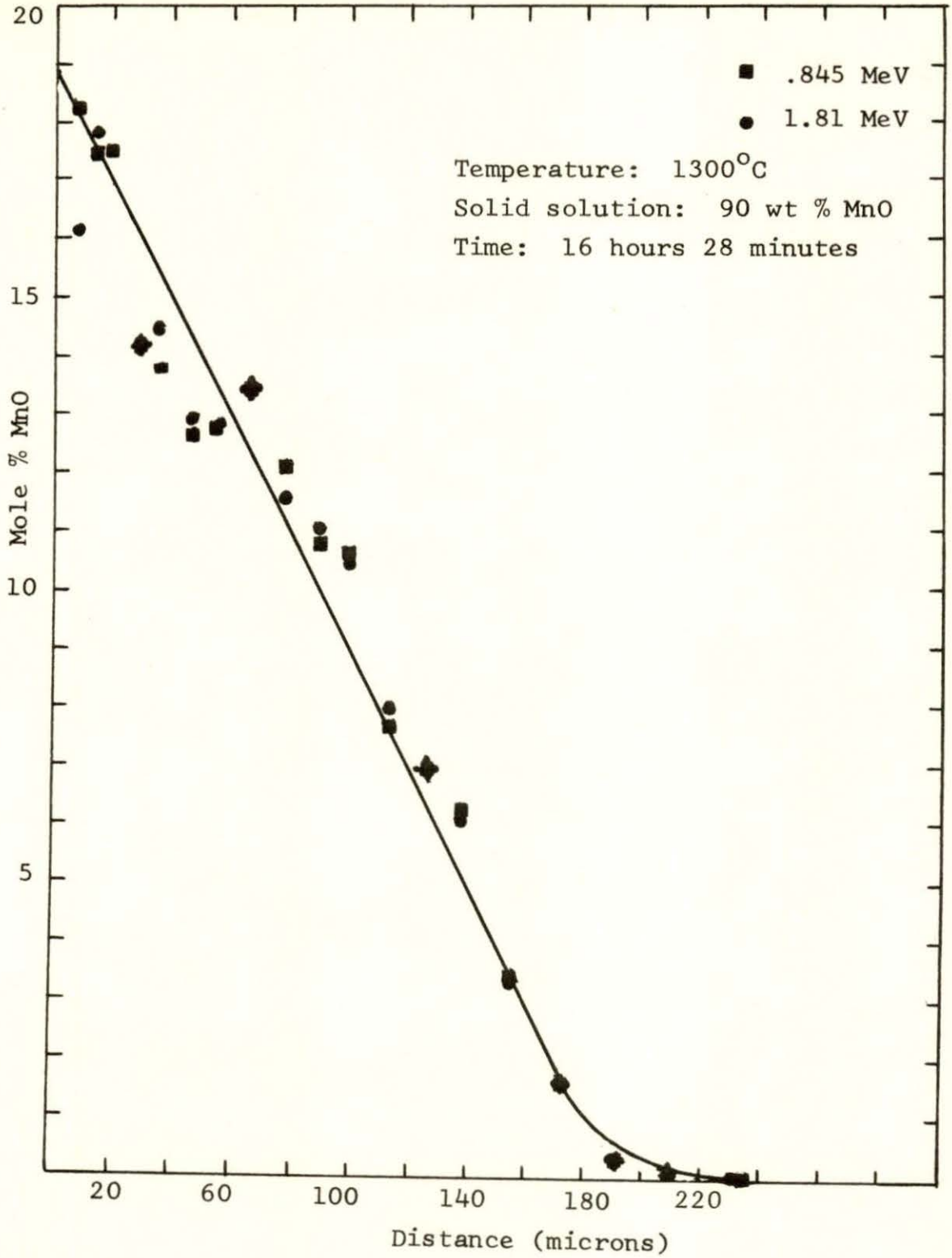

Figure 29. Concentration profile of MnO in single crystal MgO for run #9

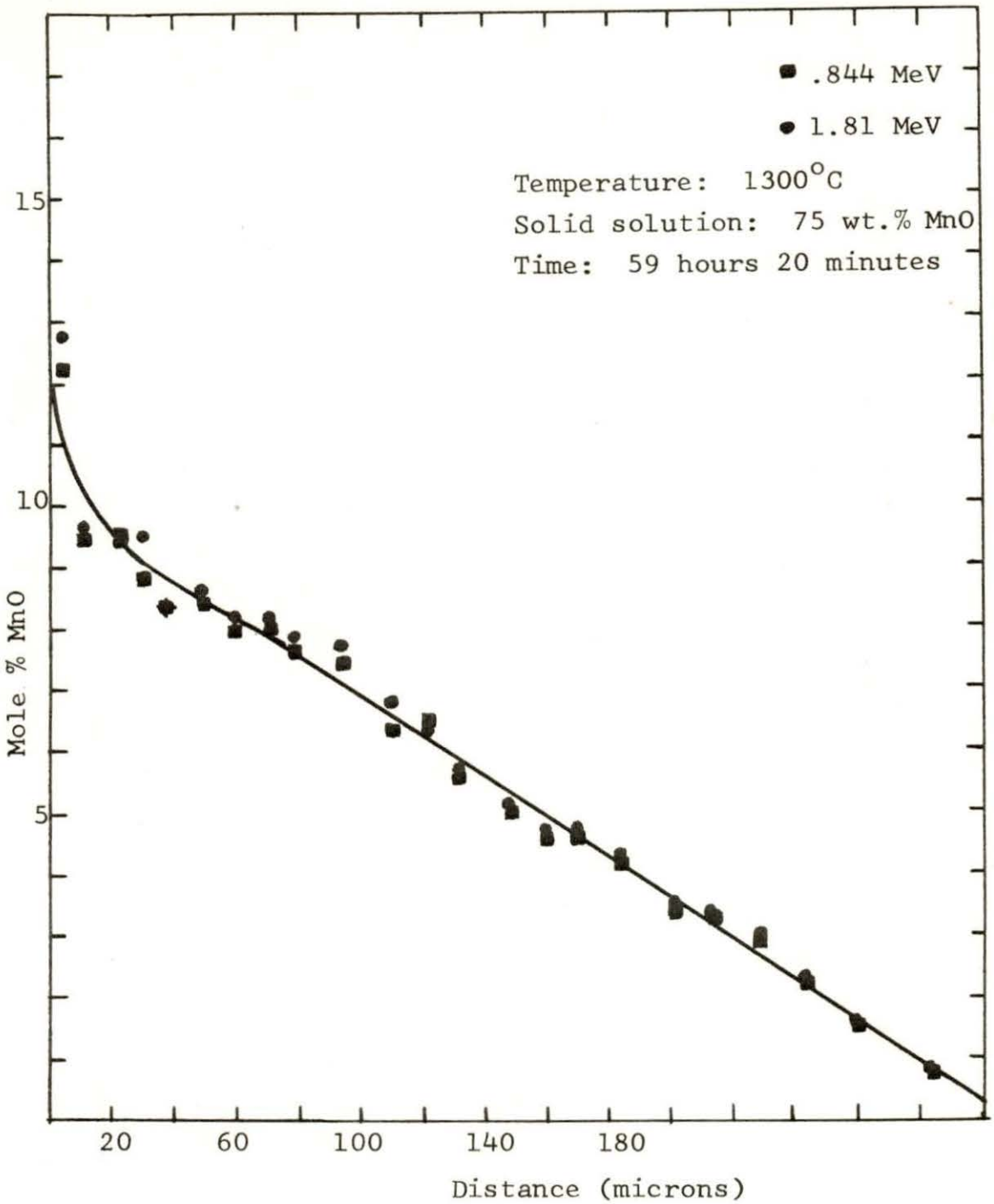

Figure 30. Concentration profile of MnO in single crystal MgO for run #11

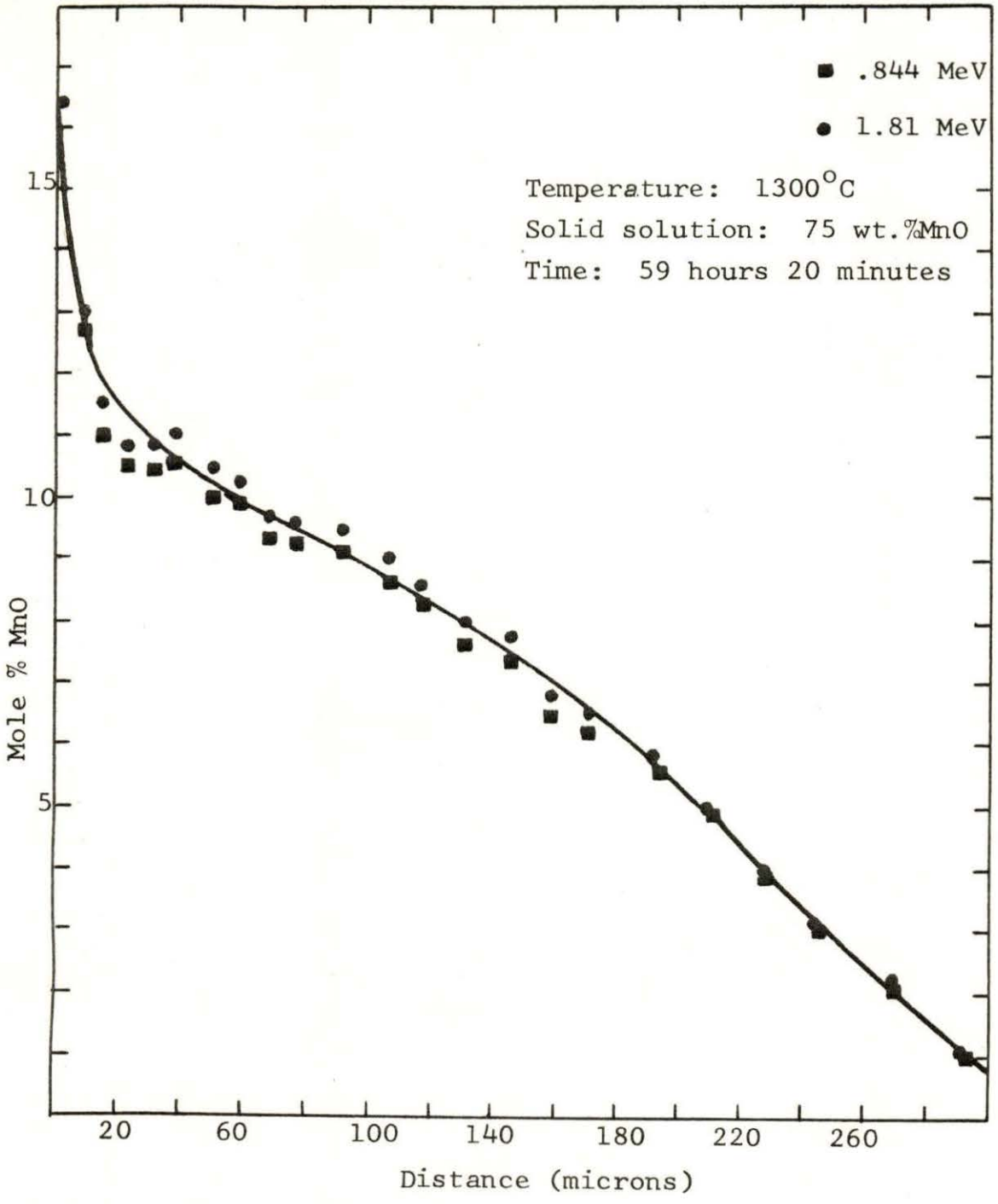

Figure 31. Concentration profile of MnO in single crystal MgO for run #12

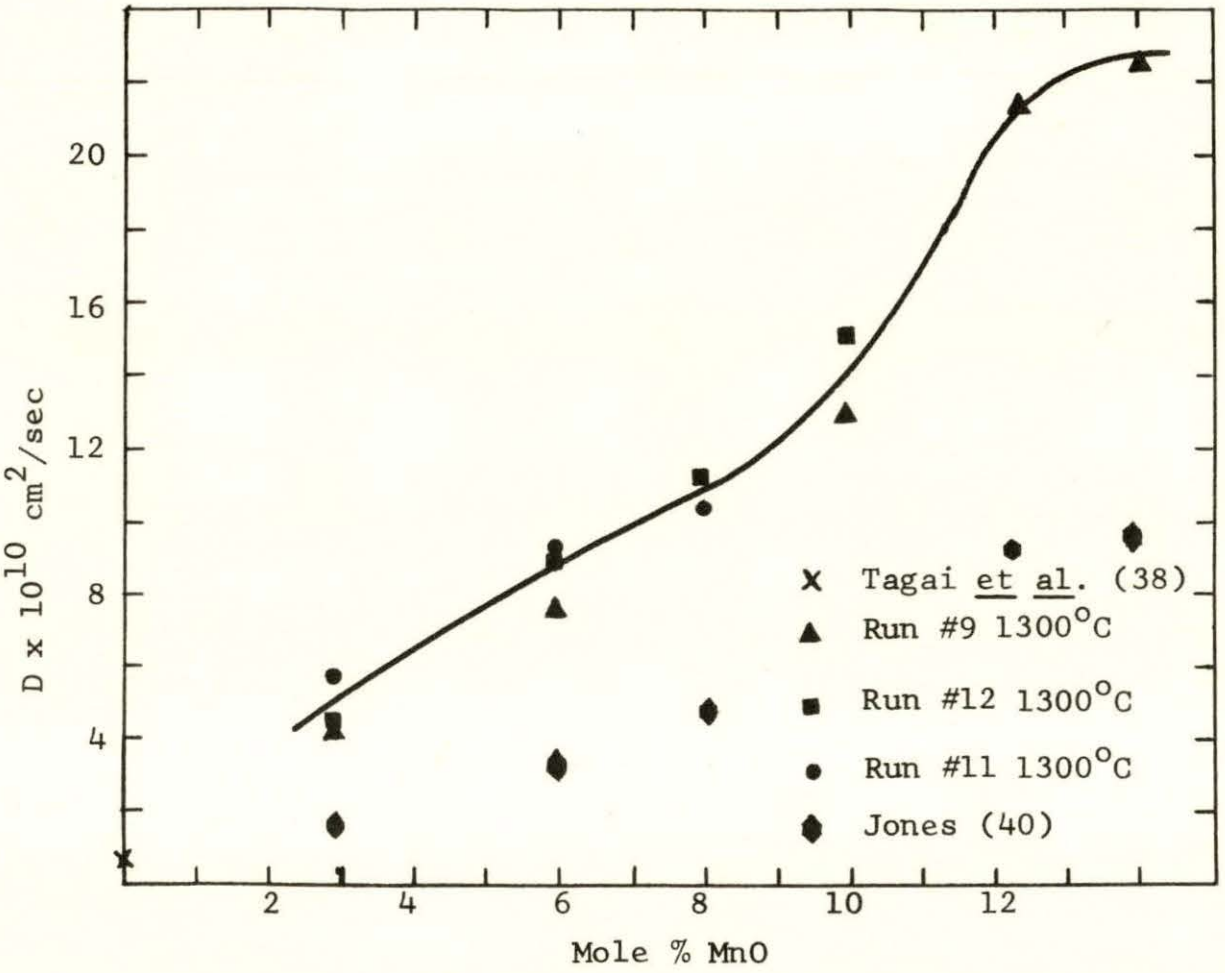

Figure 32. Plot of interdiffusion coefficient vs. mole % MnO
Note: Jones' data were taken at 1380°C and this author converted the values to correspond to 1300°C using the Arrhenius equation

VII. DISCUSSION

When this investigation was begun, it was felt that a comparison technique could be used in determining the thickness of each section which was taken off of the diffused crystal. The crystals were sectioned in the manner which was described above. A pure magnesium oxide single crystal of known dimensions was irradiated along with the diffused sample and was used as a standard for determining the thickness of each section by determining the amount of magnesium present in the section. The problem encountered was that the magnesium full-energy peaks could not be seen in the gamma spectrum of each section due to the large concentration of manganese present. Therefore the normalization technique could not be applied to the system Mn_xO-MgO.

It was then decided to determine the thickness of each section by weighing them. This technique is explained in the section on data analysis.

The cross-sectional areas of the magnesium oxide crystals in the preliminary work were small (i.e., 0.327 x 0.481 cm^2) and since it was desired to take rather thin sections off of the crystal each time (i.e., 3-5 microns) the weight of the sections were of the order of 0.5 milligram/section. Since the error in weighing such small amounts is large, it was decided to use much larger crystals (i.e., 1.38 x 1.33 cm^2) for the main experimental investigation.

In the preliminary work there was a large scattering of points to a depth of 40 to 50 microns which can be seen on the profile for run #8 (Figure 28). Since during preparation of the magnesium oxide crystals it was necessary to grind on them, it was felt that the crystals may have been damaged. An article by Koepke and Stokes (53) shows that grinding does damage the surface and subsurface of magnesium oxide crystals. Therefore for runs 11 and 12, before the diffusion anneal was carried out, the crystals were annealed for 24 hours at 1300°C in an attempt to correct any defects that may have been caused by surface grinding.

Also, as mentioned in the section on preparation of manganese standard, investigations were carried out on the effect of using either a liquid standard or a dry standard. It was found that it made no difference which type of standard was used.

The main experimental work consists of runs #9, 11, and 12. Run #10 was to be included but a malfunction in the electric furnace during the diffusion anneal caused the temperature to decrease from 1300°C to 1180°C at the start of the 16 hour run. The interdiffusion coefficients obtained from runs #9, 11, and 12 agree reasonably well with each other as can be seen in Figure 32. The results also agree reasonably well with those obtained by Jones (40) and Tagai et al. (38) as plotted on Figure 32. It is to be noted that Jones' work was carried out at 1380°C rather than the 1300°C used for runs 9-12.

As mentioned earlier, in the section on the selection of the full-energy peak, both the peak at 845 KeV and 1810 KeV were used to analyze for the manganese concentration present in the section. Figures 28, 29, 30, and 31 show that the two determinations agree very well.

The sources of error which could effect the precision of the determined interdiffusion coefficients obtained in this work are:

1) Impurities present in the magnesium oxide crystals.
2) Loss of contact between the crystal and the solid solution pellet.

and 3) Uncertainties introduced by the equipment and techniques employed in the experimental work. The nature of these uncertainties is such that their probable values can be estimated as shown in the following chapter on error analysis.

General Electric magnesium oxide single crystals were used in this investigation. These are the same crystals which were used by Romberg (17), who found the following impurities and their concentrations in parts per million: manganese < 10 ppm; copper < 1 ppm; chromium < 10 ppm; iron < 100 ppm; cobalt < 1 ppm; and scandium < 1 ppm. With such low impurity concentrations there would be negligible effect on the interdiffusion coefficients.

The loss of contact between the magnesium oxide crystal and the solid solution pellet could cause considerable error in the determination of the interdiffusion coefficients. The solid solution pellets were sintered to densify the solid solution and platinum wire or sheeting was used to hold the diffusion couple together, but loss of contact could still have occurred.

The conclusions to be drawn from this work are that activation analysis can be applied to the study of diffusion in ceramics and that the deduced interdiffusion coefficients shown in Figure 32 agree well with the results obtained by others.

VIII. ERROR ANALYSIS

An error analysis was carried out on this work and is given in detail in this chapter. Since the comparitor method was used in the determination of the amount of manganese present many possible errors tend to cancel. These were mentioned in the section on quantitative analysis.

There are several other possible sources of error and among these are the following: a) Flux variations, the sample and standards were placed as close together as possible when the irradiations were carried out so as to reduce any error caused by possible spacial flux variations; b) counting time, a possible error could result due to "dead" time but since the sections and standards had nearly the same manganese concentration, these errors would tend to cancel; c) contamination, the crystals and standards were thoroughly cleaned as outlined in the section on preparation of sample before irradiation; d) possible self-shielding errors, since the matrix crystal is MgO (which has essentially no self-shielding effect) self-shielding is negligible for the crystal, and since there was a very small amount of manganese standard, self-shielding in the standards was also considered negligible.

Other uncertainties whose values can be estimated are calculated in the following error analysis.

The propagation of errors theory (54) is first applied to the equations used in the data analysis to give the relative

errors for the values sought and finally a sample calculation is carried out using the data from run #11, section #4. These calculations are given below. The relative error associated with the basic radioactive decay equation:

$$Q_o = Q\, e^{\lambda t} \tag{36}$$

where

Q_o = total counts in full energy peak at .845 MeV for ^{56}Mn at the end of irradiation.

Q = total counts in full energy peak at .845 MeV for ^{56}Mn at time t.

t = time after irradiation (decay time) minutes

λ = decay constant of the ^{56}Mn minutes^{-1}

$$\ln Q_o = \ln Q + \lambda t$$

is

$$\frac{\Delta Q_o}{Q_o} = \sqrt{\left(\frac{\Delta Q}{Q}\right)^2 + \left(\lambda \Delta t\right)^2 + \left(t \Delta \lambda\right)^2} \tag{37}$$

Applying the propagation of errors theory to equation 23 the following relative error is obtained.

$$\frac{\Delta \text{wt. Mn}_x}{\text{wt. Mn}_x} = \sqrt{\left(\frac{\Delta \text{wt. Mn}_s}{\text{wt. Mn}_s}\right)^2 + \left(\frac{\Delta Q_{o_x}}{Q_{o_x}}\right)^2 + \left(\frac{\Delta Q_{o_s}}{Q_{o_s}}\right)^2} \tag{38}$$

where the subscripts x and s refer to the section and standard respectively.

Similar procedures are now carried out on all equations which were used in determining the required results in the data analysis section.

For each of the equations used, only the relative errors obtained from the application of the propagation of errors theory are given along with the equations.

$$\text{wt. oxygen} = \text{wt. Mn}\left(\frac{\text{atomic wt. oxygen}}{\text{atomic wt. Mn}}\right) \tag{39}$$

$$\frac{\Delta\text{wt. oxygen}}{\text{wt. oxygen}} = \sqrt{\left(\frac{\Delta\text{wt. Mn}}{\text{wt. Mn}}\right)^2 + \left(\frac{\Delta\text{atomic wt. oxygen}}{\text{atomic wt. oxygen}}\right)^2 + \left(\frac{\Delta\text{at. wt.Mn}}{\text{at. wt.Mn}}\right)^2} \tag{40}$$

$$\text{wt. MnO} = \text{wt. Mn} + \text{wt. oxygen} \tag{41}$$

$$\frac{\Delta\text{wt. MnO}}{\text{wt. MnO}} = \sqrt{\frac{(\Delta\text{wt. Mn})^2 + (\Delta\text{wt. oxygen})^2}{(\text{wt. Mn} + \text{wt. oxygen})^2}} \tag{42}$$

$$\text{wt. MgO} = \text{wt. section} - \text{wt. MnO} \tag{43}$$

$$\frac{\Delta\text{wt. MgO}}{\text{wt. MgO}} = \sqrt{\frac{(\Delta\text{wt. section})^2 + (\Delta\text{wt. MnO})^2}{(\text{wt. section} - \text{wt. MnO})^2}} \tag{44}$$

$$\text{wt. fraction MnO} = \frac{\text{wt. MnO}}{\text{wt. section}} \tag{45}$$

$$\frac{\Delta\text{wt. fraction MnO}}{\text{wt. fraction MnO}} = \sqrt{\left(\frac{\Delta\text{wt. MnO}}{\text{wt. MnO}}\right)^2 + \left(\frac{\Delta\text{wt. section}}{\text{wt. section}}\right)^2} \tag{46}$$

$$\text{molecules MnO} = \text{wt. MnO}\left(\frac{\eta_o}{\text{M. wt. MnO}}\right) \tag{47}$$

$$\frac{\Delta\text{molecules MnO}}{\text{molecules MnO}} = \sqrt{\left(\frac{\Delta\text{wt. MnO}}{\text{wt. MnO}}\right)^2 + \left(\frac{\Delta\text{M.wt. MnO}}{\text{M.wt. MnO}}\right)^2 + \left(\frac{\Delta\eta_o}{\eta_o}\right)^2} \tag{48}$$

$$\text{molecules MgO} = \text{wt. MgO}\left(\frac{\eta_o}{\text{M. wt. MgO}}\right) \tag{49}$$

$$\frac{\Delta\text{molecules MgO}}{\text{molecules MgO}} = \sqrt{\left(\frac{\Delta\text{wt. MgO}}{\text{wt. MgO}}\right)^2 + \left(\frac{\Delta\text{M.wt. MgO}}{\text{M.wt. MgO}}\right)^2 + \left(\frac{\Delta\eta_o}{\eta_o}\right)^2} \tag{50}$$

$$\#\text{unit cells/section} = \frac{\text{molecules MgO} + \text{molecules MnO}}{4} \tag{51}$$

$$\frac{\Delta\#\text{unit cells/section}}{\#\text{unit cells/section}} = \sqrt{\frac{(\Delta\text{molecules MgO})^2 + (\Delta\text{molecules MnO})^2}{(\text{molecules MgO} + \text{molecules MnO})^2}} \tag{52}$$

$$\text{Thickness section} = \frac{(\text{volume unit cell})(\#\text{ unit cells})}{\text{cross-sectional area crystal}} \tag{53}$$

$$\frac{\Delta\text{thickness}}{\text{thickness}} = \sqrt{\left(\frac{\Delta\text{vol.unit cell}}{\text{vol.unit cell}}\right)^2 + \left(\frac{\Delta\#\text{unit cells}}{\#\text{unit cells}}\right)^2 + \left(\frac{\Delta L}{L}\right)^2 + \left(\frac{\Delta W}{W}\right)^2} \tag{54}$$

The volume of a unit cell is obtained from the lattice parameter.

$$\text{Volume unit cell} = (\text{lattice parameter})^3 \tag{55}$$

The lattice parameter is obtained from the plot of the lattice parameter vs. wt. % MnO. There were no published deviations

for the values used in obtaining the plot so the error used is the error in the value of the wt. % MnO (see Figure 27, page 74).

$$\frac{\Delta \text{vol. unit cell}}{\text{vol. unit cell}} = \sqrt{3\left(\frac{\Delta \text{lattice parameter}}{\text{lattice parameter}}\right)^2} \qquad (56)$$

$$= \sqrt{3}\left(\frac{\Delta \text{lattice parameter}}{\text{lattice parameter}}\right)$$

A sample calculation is now carried out using the data obtained for section number 4 of run #11 beginning with equation 37 for the section where

Q section = 207501.5 counts for 200 seconds

t = 856.1 minutes.

Δt was given a value of $\pm$ 1 minute since the timer used to determine the decay time between the end of the irradiation and beginning of the counting was not the same as the clock used to time the end of the irradiation but the counting timer was synchronized with the clock used to time the end of the irradiation so that the decay time could be obtained. The timer read in divisions of one hundredth of one minute therefore the error in reading the timer was negligible.

All constants used were given an error value of $\pm$ 1/2 of the last significant figure unless otherwise stated.

$\lambda_{Mn} = 4.48 \times 10^{-3}$ minutes^{-1}

Half-life $^{56}Mn = t_{1/2} = 2.576 \pm .0005$ hours $= 154.56 \pm .03$ min.

$$\Delta\lambda = \frac{\lambda \Delta t_{1/2}}{t_{1/2}} = \frac{(.693)(.03)}{(154.56)^2} = 8.7 \times 10^{-7} \text{ min}^{-1}$$

$$\frac{\Delta Q_o \text{ section}}{Q_o \text{ section}} = \sqrt{\frac{1}{207501.5} + (4.48 \times 10^{-3} \times 1)^2 + (856.1 \times 8.7 \times 10^{-7})^2}$$

$$= \sqrt{4.82 \times 10^{-6} + 2.02 \times 10^{-5} + 5.55 \times 10^{-7}}$$

$$= \sqrt{25.575 \times 10^{-6}}$$

$$= 5 \times 10^{-3}$$

The factors which go into the determination of Δwt. Mn_s are the following:

1) weighing out the MnO_2 which is used as the standard.

2) making up the Mn solution - 1000 ml.

3) pipetting the solution - 1 ml.

The solution was made up so that the concentration was 1×10^{-4} grams Mn/ml solution, therefore in 1000 ml of the standard solution there was the equivalent of 0.1 g manganese. The weight of MnO_2 used to prepare this solution was 0.1582 grams.

The accuracy of the balance used was $\pm$ 0.05 mg, therefore

$$\text{wt. } MnO_2 \pm \Delta\text{wt. } MnO_2 = (\text{wt. total} - \text{wt. paper}) \pm \sqrt{(\Delta\text{wt. paper})^2 + (\Delta\text{wt. paper})^2}$$

$$= 158.2 \pm \sqrt{(.05)^2 + (.05)^2}$$

$$= 158.2 \pm 0.07\text{mg}$$

Weight Mn in standard stock solution with its Δwt.

$$\text{wt. Mn} \pm \Delta\text{wt. Mn} = (\text{wt. } MnO_2)\left(\frac{\text{M.wt.Mn}}{\text{M.wt.}MnO_2}\right)\left(1 \pm \sqrt{\left(\frac{\Delta\text{wt. } MnO_2}{\text{wt. } MnO_2}\right)^2 + \left(\frac{\Delta\text{M.W.}}{\text{M.W.}}\right)^2_{Mn} + \left(\frac{\Delta\text{M.W.}}{\text{M.W.}}\right)^2_{MnO_2}}\right)$$

$$= 158.2\left(\frac{54.94}{86.94}\right)\left(1 \pm \sqrt{\left(\frac{.0707}{158.2}\right)^2 + \left(\frac{.0005}{54.938}\right)^2 + \left(\frac{.005}{86.94}\right)^2}\right)$$

$$= 100\left(1 \pm \sqrt{(4.465 \times 10^{-4})^2 + (.912 \times 10^{-5})^2 + (.576 \times 10^{-4})^2}\right)$$

$$= 100 \pm 100\sqrt{19.92 \times 10^{-8} + .833 \times 10^{-10} + .332 \times 10^{-8}}$$

$$= 100 \pm 100\sqrt{20.26 \times 10^{-8}}$$

$$= 100 \pm 100\,(4.505 \times 10^{-4})$$

$$= 100.0 \pm 0.05 \text{ mg Mn in standard}$$

To make up the standard solution, 1000 ml volumetric flask with accuracy of $\pm$ .3 ml was used. Since human error enters into accuracy when pipetting, a value of 1% error was included.

As mentioned earlier, standards containing 1.00×10^{-4} grams of manganese were used in run #11, therefore 1 ml of stock solution was pipetted.

Weight manganese in final standard:

$$\text{wt. } Mn_{STD} \pm \Delta\text{wt. } Mn_{STD} = \text{wt. } Mn\left(\frac{\text{Final vol.}}{\text{stock sol.}}\right)\left(1 \pm \sqrt{\left(\frac{\Delta wt}{wt}\right)^2 + \left(\frac{\Delta vol.}{vol.}\right)^2_{stock} + \left(\frac{\Delta vol.}{vol.}\right)^2_{final}}\right)$$

$$= (100 \text{ mg}) \quad \frac{1 \text{ ml}}{1000 \text{ ml}} \left(1 \pm \sqrt{\left(\frac{.04505}{100}\right)^2 + \left(\frac{.3 \text{ ml}}{1000 \text{ ml}}\right)^2 + \left(\frac{.01}{1}\right)^2}\right)$$

$$= .1 \text{ mg} \pm .1\sqrt{(4.505 \times 10^{-4})^2 + (3 \times 10^{-4})^2 + (1 \times 10^{-2})^2}$$

$$= .1 \text{ mg} \pm .1\sqrt{20.26 \times 10^{-8} + 9 \times 10^{-8} + 10^{-4}}$$

$$= .1 \pm .1\,(.01) \text{ mg} = 0.100 \pm 0.001 \text{ mg}$$

$$= (1.00 \pm .01) \times 10^{-4} \text{ grams manganese.}$$

Determination of $\Delta Q_{o_s} / Q_{o_s}$ same as for the section except for

$Q_s = 318928.0$

$t = 356.8$ minutes

$$\frac{\Delta Q_{o_s}}{Q_{o_s}} = \sqrt{\frac{1}{318928.0} + 2.02 \times 10^{-5} + (8.7 \times 10^{-7} \times 356.8)^2}$$

$$= \sqrt{3.138 \times 10^{-6} + 2.02 \times 10^{-5} + 9.64 \times 10^{-7}}$$

$$\frac{\Delta Q_{o_s}}{Q_{o_s}} = 5 \times 10^{-3}$$

$$\frac{\Delta \text{wt. Mn}_x}{\text{wt. Mn}_x} = \sqrt{\left(\frac{.01 \times 10^{-4}}{1.0 \times 10^{-4}}\right)^2 + (5.045 \times 10^{-3})^2 + (5 \times 10^{-3})^2}$$

$$= \sqrt{4 \times 10^{-4} + .25575 \times 10^{-4} + .24302 \times 10^{-4}}$$

$$\frac{\Delta \text{wt. Mn}_x}{\text{wt. Mn}_x} = 1 \times 10^{-2}$$

For the determination of Δwt. oxygen/wt. oxygen the atomic weight of oxygen and manganese are required:

Atomic weight oxygen = $15.9994 \pm .00005$

Atomic weight manganese = $54.9380 \pm .00005$.

$$\frac{\Delta \text{wt. oxygen}}{\text{wt. oxygen}} = \sqrt{(1 \times 10^{-2})^2 + \left(\frac{.00005}{15.9994}\right)^2 + \left(\frac{.00005}{54.9380}\right)^2}$$

$$= \sqrt{1 \times 10^{-4} + 9.76 \times 10^{-12} + 8.3 \times 10^{-13}}$$

$$\frac{\Delta \text{wt. oxygen}}{\text{wt. oxygen}} = 1 \times 10^{-2}$$

$$\frac{\Delta \text{wt.MnO}}{\text{wt.MnO}} = \sqrt{\frac{(\text{wt.Mn})^2\left[\left(\frac{\Delta \text{wt.Mn}}{\text{wt.Mn}}\right)^2 + \left(\frac{\Delta \text{wt.oxygen}}{\text{wt.oxygen}}\right)^2 \left(\frac{\text{at.wt.oxygen}}{\text{at.wt.Mn}}\right)^2\right]}{(\text{wt. Mn})^2\left[1 + \left(\frac{\text{at.wt.oxygen}}{\text{at.wt.Mn}}\right)\right]^2}}$$

$$= \sqrt{\frac{\left[(1 \times 10^{-2})^2 + (1 \times 10^{-2})^2 \left(\frac{15.9994}{54.938}\right)^2\right]}{\left[1 + \left(\frac{15.9994}{54.938}\right)\right]^2}}$$

$$= \sqrt{\frac{1 \times 10^{-4} + 1 \times 10^{-5}}{1.669}}$$

$$\frac{\Delta \text{wt. MnO}}{\text{wt. MnO}} = 1 \times 10^{-2}$$

$$\frac{\Delta \text{wt. MgO}}{\text{wt. MgO}} = \sqrt{\frac{(\Delta \text{wt. section})^2 + (\Delta \text{wt. MnO})^2}{(\text{wt. section} - \text{wt. MnO})^2}}$$

The weight of each section was determined using a Cahn electrobalance. In run #11 the scale was equal to 40 milligrams full scale. The accuracy of the balance is $\pm$ .0005, therefore, on 40 milligrams full scale Δwt. = $\pm$ 0.00002 grams. Since the sections were weighed by the difference method Δwt. section = $\pm$ .00004.

$$\frac{\Delta \text{wt. MgO}}{\text{wt. MgO}} = \sqrt{\frac{(4 \times 10^{-5})^2 + (1 \times 10^{-2} \times .786 \times 10^{-3})^2}{(5.44 \times 10^{-3} - .786 \times 10^{-3})^2}}$$

$$= \sqrt{\frac{1.6 \times 10^{-9} + 6 \times 10^{-11}}{2.16 \times 10^{-5}}}$$

$$\frac{\Delta \text{wt. MgO}}{\text{wt. MgO}} = 8 \times 10^{-3}$$

$$\frac{\Delta \text{wt. fraction MnO}}{\text{wt. fraction MnO}} = \sqrt{\left(\frac{\Delta \text{wt. MnO}}{\text{wt. MnO}}\right)^2 + \left(\frac{\Delta \text{wt. section}}{\text{wt. section}}\right)^2}$$

$$= \sqrt{1 \times 10^{-4} + \left(\frac{4 \times 10^{-5}}{5.44 \times 10^{-3}}\right)^2}$$

$$\frac{\Delta \text{wt. fraction MnO}}{\text{wt. fraction MnO}} = 1 \times 10^{-2}$$

The lattice parameter was obtained from a plot of the lattice parameter vs. the wt. % MnO. The data which was used in the plot did not have an error value with it so that the error in the lattice parameter value is obtained from the error in the wt. % MnO.

$$\Delta \text{wt. fraction MnO} = \frac{\Delta \text{wt. fraction MnO}}{\text{wt. fraction MnO}} \left(\frac{\text{wt MnO}}{\text{wt. section}}\right)$$

$$= (1 \times 10^{-2}) \left(\frac{\text{wt MnO}}{5.44 \times 10^{-3}}\right)$$

$$= (1 \times 10^{-2})(.144)$$

Δwt. fraction MnO = 1×10^{-3}

Therefore wt % MnO = $14.4 \pm .1$

$$\Delta X = .1$$

from graph

$$\Delta Y = .0002$$

Volume of each unit cell in section:

Volume unit cell = Y^3 Y = lattice parameter

$$\frac{\Delta Vol}{Vol} = \sqrt{3\left(\frac{\Delta Y}{Y}\right)^2} = \sqrt{3}\,\frac{\Delta Y}{Y} = 1.732\left(\frac{.0002}{4.224}\right)$$

$$\frac{\Delta Vol}{Vol} = 8 \times 10^{-5}$$

$$\frac{\Delta \text{molecules MnO}}{\text{molecules MnO}} = \sqrt{\left(\frac{\Delta \text{wt. MnO}}{\text{wt. MnO}}\right)^2 + \left(\frac{\Delta \text{M. wt. MnO}}{\text{M. wt. MnO}}\right)^2 + \left(\frac{\Delta \eta_o}{\eta_o}\right)^2}$$

$\eta_o = (6.02252 \pm .00028) \times 10^{23}$

$$= \sqrt{(1.0 \times 10^{-2})^2 + \left(\frac{.0005}{70.937}\right)^2 + \left(\frac{.00028}{6.02252}\right)^2}$$

$$= \sqrt{1.0 \times 10^{-4} + 5. \times 10^{-11} + 2.2 \times 10^{-9}}$$

$$\frac{\Delta \text{molecules MnO}}{\text{molecules MnO}} = 1 \times 10^{-2}$$

$$\frac{\Delta \text{molecules MgO}}{\text{molecules MgO}} = \sqrt{\left(\frac{\Delta \text{wt. MgO}}{\text{wt. MgO}}\right)^2 + \left(\frac{\Delta \text{mol. wt. MgO}}{\text{mol. wt. MgO}}\right)^2 + \left(\frac{\Delta \eta_o}{\eta_o}\right)^2}$$

$$= \sqrt{6 \times 10^{-5} + \left(\frac{.0005}{40.311}\right)^2 + \left(\frac{.00028}{6.02252}\right)^2}$$

$$= \sqrt{6 \times 10^{-5} + 1.539 \times 10^{-10} + 2.2 \times 10^{-9}}$$

$$\frac{\Delta \text{molecules MgO}}{\text{molecules MgO}} = 8 \times 10^{-3}$$

$$\frac{\Delta \#\text{unit cells/section}}{\#\text{unit cells/section}} = \sqrt{\frac{(\Delta \text{molecules MgO})^2 + (\Delta \text{molecules MnO})^2}{(\text{molecules MgO} + \text{molecules MnO})^2}}$$

$$= \sqrt{\frac{[(8 \times 10^{-3})(4.654 \times 10^{-3})\left(\frac{6.02252 \times 10^{23}}{40.311}\right)]^2 + [(1 \times 10^{-2}) \times (.786 \times 10^{-3})\left(\frac{6.02252 \times 10^{23}}{70.938}\right)]^2}{[(4.654 \times 10^{-3})\left(\frac{6.02252 \times 10^{23}}{40.311}\right) + (.786 \times 10^{-3})\left(\frac{6.02252 \times 10^{23}}{70.938}\right)]^2}}$$

$$= \sqrt{\frac{8 \times 10^{-13} + 1 \times 10^{-14}}{1.0 \times 10^{-8}}}$$

$$\frac{\Delta \#\text{unit cells/section}}{\#\text{unit cells/section}} = 7 \times 10^{-3}.$$

$$\frac{\Delta \text{thickness}}{\text{thickness}} = \sqrt{\left(\frac{\Delta \text{vol.unit cell}}{\text{vol.unit cell}}\right)^2 + \left(\frac{\Delta \#\text{unit cells}}{\#\text{unit cells}}\right)^2 + \left(\frac{\Delta L}{L}\right)^2 + \left(\frac{\Delta W}{W}\right)^2}$$

The length and width of the crystals were measured using a micrometer with an accuracy of $\pm$ 0.0002 therefore the dimensions of the crystal in run #11 are

$$L = 1.4346 \pm .0002$$

$$W = 1.20218 \pm .0002$$

$$\frac{\Delta \text{thickness section}}{\text{thickness section}} = \sqrt{(8 \times 10^{-5})^2 + \left(\frac{.0002}{1.4346}\right)^2 + \left(\frac{.0002}{1.20218}\right)^2 + (7 \times 10^{-3})^2}$$

$$= \sqrt{6 \times 10^{-9} + 1.94 \times 10^{-8} + 2.76 \times 10^{-8} + 5 \times 10^{-5}}$$

$$= \sqrt{49 \times 10^{-6}}$$

$$\frac{\Delta \text{thickness section}}{\text{thickness section}} = 7 \times 10^{-3}$$

IX. SUGGESTIONS FOR CONTINUING WORK

Several problems were encountered during this investigation. The foremost was the difficulty of making certain that the solid solution and the crystal were in complete contact during the diffusion anneal. Further work should be done in finding a way to make certain these are in contact. Another important problem is whether the Boltzmann-Matano interface is the original interface. A method which could be used in finding this out would be to use a MnO single crystal in place of the solid solution, and then analyze the MnO crystal in the same manner as the MgO crystal. In this way the whole diffusion profile could be obtained, rather than only the profile from the MgO crystal.

The technique which was used in this investigation should also be applied to other diffusion couple systems.

X. LITERATURE CITED

1. Hevesy, G. and Levi H. The action of neutrons on the rare earth elements. Kgl. Danske Videnskab. Selskab, Math-fys. Medd. 14, 5: 1936.

2. Seaborg, G. T. and Livingood, J. J. Artificial radioactivity as a test for minute traces of elements. J. Am. Chem. Soc. 60: 1784-1786. 1938.

3. Lutz, G. J., Boreni, R. J., Maddock, R. S. and Meinke, W. W., editors. Activation analysis: a bibliography. Nat. Bur. Std. Technical Note 467.

4. Roberts, D. M., Whitmer, S. and Nieman, W. References related to activation analysis. Iowa State University Project Themis Ceramic Materials Report ISU-ERI-Ames-80600. 1970.

5. Koch, R. C. Activation analysis handbook. New York, N.Y., Academic Press Inc. 1960.

6. Lenihan, J. M. A. and Thomson, S. J., editors. Activation analysis, principles and application. New York, N.Y., Academic Press Inc. 1965.

7. Lyon, William, editor. Guide to activation analysis. Princeton, N.J., D. Van Nostrand Co., Inc. 1964.

8. Brown, Mildred W., editor. International Conference on Modern Trends in Activation Analysis 1961 Proceedings. Activation Analysis Research Laboratory Texas A&M University, College Station, Texas. 1961.

9. Guinn, John P., editor. International Conference on Modern Trends in Activation Analysis 1965 Proceedings. Activation Analysis Research Laboratory Texas A&M University, College Station, Texas. 1965.

10. DeVoe, James P., editor. International Conference on Modern Trends in Activation Analysis 1968 Proceedings. National Bureau of Standards Special Publication 312, Vol. 1. 1969.

11. DeVoe, James P., editor. International Conference on Modern Trends in Activation Analysis 1968 Proceedings. National Bureau of Standards Special Publication 312, Vol. 2. 1969.

12. Payne, Bryan R. Radioactivation Analysis Symposium 1959 Proceedings. London, England, Butterworth and Co., Ltd. 1960.

13. Voigt, A. F. and Abu-Samra, A. Analysis of a Damascus steel by neutron and gamma activation. International Conferences on Modern Trends in Activation Analysis 1965 Proceedings: 22-25. 1965.

14. Kawashima, Toshi. Determination of impurities in high-purity niobium and tantalum by radioactivation analysis. International Conference on Modern Trends in Activation Analysis 1965 Proceedings: 61-65. 1965.

15. Rojas, M. A., Dyer, I. A. and Cassatt, W. A. Determination of manganese in bone by neutron activation analysis. Anal. Chem. 38: 788-789. 1966.

16. Bate, L. C. and Dyer, F. F. Trace elements in human hair. Nucleonics 23, 10: 74-81. 1965.

17. Romberg, Wayne D. Impurities in MgO by instrumental neutron activation analysis. Unpublished M.S. thesis. Ames, Iowa, Library, Iowa State University. 1969.

18. Lee, Hee Myong. Determination of impurities in single crystals of magnesium oxide by neutron activation analysis. Analytica Cheimica Acta. 41: 431-440. 1968.

19. Ryskin, G. Y. Diffusion coefficient measurement by the radioactivation analysis and isotopic dilution methods. Soc. Phys. Solid State 1, 6: 870-872. 1959.

20. Leliaert, G. Determination of trace element diffusion in quartz and in germanium. Pure and Appl. Chem. 1, 1: 121-126. 1960.

21. Ascoli, A. and Germagnoli, E. Intermetallic diffusion in gold-lead systems. Pure and Appl. Chem. 1, 1: 139-141. 1960.

22. Jaumot, F. E., Jr. A bibliography of diffusion of gases, liquids, and solids in solids, 1890 to 1955. U.S. Atomic Energy Commission Report TI-3071 [Division of Technical Information Extension, AEC]. 1958.

23. Berard, Michael F. Diffusion in ceramic systems; a selected bibliography. U.S. Atomic Energy Commission Report IS-448 [Iowa State University, Ames, Inst. for Atomic Research]. 1962.

24. Wachtman, J. B. and Franklin, A. D., editors. Mass transport in oxides. National Bureau of Standards Special Publication 296. 1968.

25. Diffusion Information Center. Diffusion data. Vol. 1. Cleveland, Ohio, author. 1967.

26. Barrer, R. M. Diffusion in and through solids. New York, N.Y., The Macmillan Co. 1941.

27. Jost, W. Diffusion in solids, liquids, gases. New York, N.Y., Academic Press Inc. 1952.

28. Shewmon, Paul G. Diffusion in solids. New York, N.Y., McGraw-Hill Book Co. 1963.

29. Manning, John R. Diffusion kinetics for atoms in crystals. New York, N.Y., D. Van Nostrand Co., Inc. 1968.

30. Crank, J. The mathematics of diffusion. Oxford, England, The Clarendon Press. 1956.

31. Rungis, J. and Mortlock, A. S. Diffusion of Ca in MgO. Philosophical Magazine 14: 821-828. 1966.

32. Harding, B. C. The diffusion of barium in magnesium oxide. Philosophical Magazine 16: 1039-1048. 1967.

33. Lindner, Roland and Parfitt, Geoffrey D. Diffusion of radioactive magnesium in magnesium oxide crystals. J. of Chem. Phys. 26, 1: 182-185. 1957.

34. Zaplatynsky, I. Diffusion of Co^{2+} and Ni^{2+} in magnesium oxide. J. Am. Cer. Soc. 45, 1: 28-31. 1962.

35. Rigby, Bertrand E. and Cutler, Ivan B. Interdiffusion studies of the system Fe_xO-MgO. J. Am. Cer. Soc. 48, 2: 95-99. 1965.

36. Wuensch, B. J. and Vasilos, T. Diffusion of Zn^{2+} in single-crystal MgO. J. of Chem. Phys. 42, 12: 4113-4115. 1965.

37. Wuensch, B. J. and Vasilos, T. Diffusion of transition metal ions in single-crystal MgO. J. of Chem. Phys. 36, 11: 2917-2922. 1962.

38. Tagai, Von H., Iwai, S., Iseki, T. and Saho, Tokoi M. Diffusion of iron manganese, and chromium oxides into single crystal magnesia. Radex-Rundshaw 4: 577-583. 1965.

39. Blank, Stuart L. and Pask, Joseph A. Diffusion of iron and nickel in magnesium oxide single crystals. J. Am. Cer. Soc. 52, 12: 669-675. 1969.

40. Jones, J. T. The diffusion of manganese oxide in single crystals of periclase. Unpublished Ph.D. thesis. Salt Lake City, Utah, Library, University of Utah. 1965.

41. Meinke, W. W. Trace-element sensitivity: comparison of activation analysis with other methods. Science 121: 177-184. 1955.

42. Meinke, W. W. Sensitivity charts for neutron activation analysis. Analytical Chemistry 31: 792.

43. Goldman, David. T. Chart of the nuclides. Schenectady, N.Y., Educational relations General Electric Co. 1964.

44. Lederer, C. M., Hollander, J. M. and Perlman, I. Table of isotopes. 6th edition. New York, N.Y., John Wiley and Sons, Inc. 1967.

45. Heath, R. L. Scintillation spectrometry, gamma-ray spectrum catalogue. 2nd edition. U.S. Atomic Energy Commission Report IDO-16880 [Idaho Operations Office, AEC]. 1964.

46. Kaplan, I. Nuclear physics. 2nd edition. Reading, Mass., Addison-Wesley Publishing Co., Inc. 1962.

47. Price, William J. Nuclear radiation detection. 2nd edition. New York, N.Y., McGraw-Hill Book Co., Inc. 1964.

48. Covell, D. F. A new method of determining photopeak areas. Analytical Chemistry 31: 1785. 1959.

49. Berard, M. F. Self-diffusion in polycrystalline yttrium oxide. Unpublished M.S. thesis. Ames, Iowa, Library, Iowa State University. 1962.

50. Riboud, P. V. and Maun, A. Melting relations of CaO-manganese oxide and MgO-manganese oxide mixtures in air. J. Am. Cer. Soc. 46, 1: 33-36. 1963.

51. Jones, John T. and Cutler, I. B. Stoichiometry of MgO-Mn_xO solid solutions in air at high temperatures. J. Am. Cer. Soc. 49, 10: 572-573. 1966.

52. Jay, A. H. and Andrew, K. W. Note on oxide system pertaining to steel-making furnace slage. J. Iron and Steel Institute 152, 2: 15-18. 1945.

53. Koepke, B. G. and Stokes, R. J. A study of grinding damage in magnesium oxide single crystals. J. Materials Science 5: 240-247. 1970.

54. Bevington, Philip R. Data reduction and error analysis for the physical sciences. New York, N.Y., McGraw-Hill Book Co., Inc. 1969.

XI. ACKNOWLEDGMENTS

The author wishes to express his appreciation to Dr. Donald M. Roberts for his helpful discussion, opinions and criticism during this investigation and especially during the preparation of this thesis.

Appreciation is also expressed to Dr. Michael Berard for the use of the sectioning device and for his assistance and discussion throughout this investigation; Drs. G. Murphy, R. A. Hendrickson, and A. F. Voigt for assisting in the author's graduate work; the Radiological Service Group of the University and the Health Physics Group at Ames Lab; Mr. Bruce Link for irradiations carried out in the Ames Lab reactor; the Ceramic Engineering Department at Iowa State University for assistance and use of their facilities; Mr. Stephen Whitmer for preparation of the computer program, the drafting work required, and assistance in analyzing the data; Miss Marilyn Sundberg for aid in preparation of this manuscript; and the ERI project Themis supported by the Aerospace Research Laboratories, Themis contract F33615-68-C-1034 for its sponsorship that has made my graduate work possible.

Finally, the author is grateful to his wife and family for their continued sacrifice and support during this work.

XII. APPENDIX A EXPERIMENTAL DATA

DATA
Run #7

Solid solution concentration = 75 wt. % MnO-25 wt. % MgO
Cross-sectional area crystal = .506 x .445 cm^2
Diffusion time = 16 hours
Diffusion temperature = 1410 ± 5°C

Thickness sections are in microns

Section number	Counts in peak 0.845 MeV	Counts in peak 1.81 MeV	Decay time minutes	Weight section Mg	Wt. % MnO 0.845 MeV	Wt. % MnO 1.81 MeV	Thickness section 0.845 MeV	Thickness section 1.81 MeV
1	10638	1150	160.2	.150	33.8	36.3	1.644	1.629
2	16339	1897	163.0	.282	30.0	30.0	3.131	3.131
3	18649	1922	165.6	.340	25.5	28.8	3.835	3.791
4	19690	1929	168.1	.518	17.0	20.2	6.013	5.949
5	18560	2098	170.6	.490	19.8	20.3	5.636	5.625
6	18227	1894	173.2	.612	14.4	16.2	7.165	7.124
7	18676	2015	175.6	.418	22.7	24.5	4.759	4.730
8	15394	1406	178.0	.416	16.1	20.5	4.843	4.772
9	23074	2163	180.4	.516	20.2	25.1	5.926	5.828
10	24260	2704	183.0	.768	17.2	18.9	8.910	8.888
11	17280	1802	185.4	.502	17.7	19.7	5.814	5.774
12	17574	2005	187.9	.628	15.9	16.2	7.316	7.309
13	16057	1766	190.4	.492	18.1	19.1	5.690	5.670
14	22338	2312	192.9	.560	21.0	23.6	6.413	6.356
15	16336	1668	195.4	.708	12.1	13.8	8.352	8.305
16	21745	2471	197.8	.884	14.6	14.9	10.34	10.33
Standard	16862	1961	200.3	.08 mg Mn				

DATA
Run #8

Solid solution concentration = 75 wt. % MnO-25 wt. % MgO
Cross-sectional area crystal = .3085 x .3548 cm^2
Diffusion time = 16 hours
Diffusion temperature = 1410 ± 5°C

Section number	Counts in peak 0.845 MeV	Counts in peak 1.81 MeV	Decay time minutes	Weight section Mg	Wt. % MnO 0.845 MeV	Wt. % MnO 1.81 MeV	Thickness section 0.845 MeV	Thickness section 1.81 MeV
1	155968	18410	224.8	.114	46.7	46.5	3.083	3.085
2	179214	21612	227.6	.360	21.7	22.1	8.426	8.415
3	201195	24711	160.8	.332	19.6	20.3	7.826	7.807
4	219130	25846	164.2	.324	22.2	22.1	7.570	7.573
5	251387	29827	167.0	.348	24.1	24.1	8.081	8.080
6	272616	32432	170.0	.404	22.8	22.9	9.422	9.419
7	260129	30373	172.9	.404	22.0	21.7	9.447	9.457
8	235754	27444	178.4	.368	22.4	22.1	8.592	8.604
9	265450	30802	181.5	.416	22.7	22.2	9.706	9.721
10	228500	26993	184.6	.428	19.2	19.2	10.10	10.10
11	221985	26071	190.7	.456	18.0	17.9	10.81	10.81
12	191710		193.2	.388	18.5		9.181	
13	194739	23151	195.7	.476	15.5	15.5	11.38	11.38
14	169983	19601	198.2	.528	12.3	12.0	12.75	12.77
15	135739	15448	200.6	.500	10.5	10.1	12.15	12.17
16	134655	14742	203.0	.742	7.1	6.6	18.23	18.26
17	59369	6997	205.3	.716	3.3	3.3	17.81	17.81
18	22908	2690	207.4	.824	1.1	1.1	20.64	20.64
19	1874	367	210.4	.566	0.1	0.2	14.22	14.22
20	479		214.6	.016	0.0		25.54	
Standard	242775	28764	221.8	.08 mg Mn				

DATA

Run #9

Solid solution concentration = 90 wt. % MnO-10 wt. % MgO

Cross-sectional area crystal = .542 x .2625 cm^2

Diffusion time = 16 hours 28 minutes

Diffusion temperature = 1300 ± 5°C

Section number	Counts in peak 0.845 MeV	Counts in peak 1.81 MeV	Decay time minutes	Weight section Mg	Wt. % MnO 0.845 MeV	Wt. % MnO 1.81 MeV	Thickness section 0.845 MeV	Thickness section 1.81 MeV
1	181063	20637	182.0	.188	36.7	35.4	3.229	3.245
2	146152	15926	185.0	.200	28.2	26.0	3.540	3.567
3	155753	18918	187.8	.190	32.1	32.9	3.318	3.308
4	164539	19791	190.8	.240	27.2	27.6	4.263	4.256
5	209484	24721	193.5	.308	27.3	27.2	5.469	5.470
6	234472	27798	196.2	.424	22.5	22.5	7.655	7.653
7	224773	27382	198.9	.418	22.1	22.8	7.555	7.539
8	260835	31417	202.5	.534	20.4	20.8	9.708	9.696
9	263039	31255	205.4	.544	20.5	20.6	9.888	9.885
10	274876	32570	208.3	.550	21.4	21.5	9.964	9.963
11	290468	33154	217.5	.664	19.5	18.9	12.11	12.13
12	226010	27286	220.6	.582	17.6	18.0	10.68	10.67
13	228620	26578	223.3	.608	17.2	16.9	11.17	11.18
14	205358	25256	226.0	.748	12.7	13.2	13.95	13.93
15	156005	18460	228.7	.628	11.7	11.7	11.75	11.75
16	151333	17918	231.3	.688	10.5	10.5	12.93	12.93
17	108571	12632	234.0	.882	5.9	5.8	16.82	16.83
18	58439	7082	236.5	1.00	2.8	2.9	19.26	19.26
19	11283	1445	239.1	.900	0.6	0.7	17.46	17.46
20	228	119	241.8	.932	0.0	0.0	18.11	18.11
21	242	138	245.8	1.176	0.0	0.0	22.86	22.85
Standard	283553	33554	171.9	.08 mg Mn				

DATA

Run #10

Solid solution concentration = 75 wt. % MnO-25 wt. % MgO

Cross-sectional area crystal = 1.364 x 1.519 cm^2

Diffusion time = 16 hours

Diffusion temperature = 1300 to 1180°C Glow bar broke

Section number	Counts in peak 0.845 MeV	1.81 MeV	Decay time minutes	Weight section Mg	Wt. % MnO 0.845 MeV	1.81 MeV	Thickness section 0.845 MeV	1.81 MeV
1	179345	21975	210.65	.852	9.0	9.5	1.192	1.190
2	194849	23407	218.5	.992	8.7	9.0	1.389	1.388
3	285165	33876	221.3	1.656	7.7	7.9	2.327	2.326
4	181364	21407	223.7	1.076	7.7	7.7	1.512	1.512
5	105781	12377	226.1	.644	7.5	7.6	9.054	9.053
6	251056	29121	228.3	1.428	8.1	8.1	2.004	2.004
7	324237	38511	230.7	1.992	7.6	7.8	2.800	2.798
8	349446	41017	233.1	2.616	6.3	6.4	3.692	3.692
9	177657	22209	236.0	1.180	7.2	7.7	1.661	1.658
10	159095	18894	238.2	1.044	7.4	7.5	1.468	1.468
11	191780	22563	240.4	1.344	7.0	7.0	1.893	1.893
12	183857	21590	242.6	1.382	6.6	6.6	1.949	1.949
13	271570	31449	245.0	1.844	7.4	7.3	2.594	2.594
14	306523	35992	247.1	2.396	6.5	6.5	3.380	3.380
15	181723	22719	249.5	1.312	7.1	7.6	1.847	1.844
16	288183	32069	251.7	2.128	7.0	6.7	2.997	3.000
17	384572	45593	254.1	2.804	7.1	7.3	3.947	3.946
18	182476	21416	256.6	1.608	6.0	6.0	2.272	2.272
19	150406	18339	258.8	1.288	6.2	6.5	1.819	1.817
Standard	294280	34335	216.0	.10 mg Mn				

DATA

Run #11

Solid-solution concentration = 75 wt. % MnO-25 wt. % MgO

Cross-sectional area crystal = 1.434 x 1.202 cm^2

Diffusion time = 59 hours 20 minutes

Diffusion temperature = 1300 ± 5°C Glow bar broke before completion

Section number	Counts in peak 0.845 MeV	1.81 MeV	Decay time minutes	Weight section Mg	Wt. % MnO 0.845 MeV	1.81 MeV	Thickness section 0.845 MeV	1.81 MeV
1	168899.5	20390	843.6	3.064	19.7	20.6	4.610	4.597
2	195917.	23108.5	847.8	4.576	15.6	15.9	6.981	6.974
3	254703.5	29646	851.9	6.160	15.4	15.4	9.405	9.403
4	207501.5	26124.5	856.1	5.440	14.4	15.7	8.331	8.296
5	176738.5	20516	860.4	4.936	13.8	13.9	7.575	7.574
6	272267.5	32602	865.0	7.720	13.9	14.3	11.84	11.83
7	240731.5	28498.5	869.2	7.320	13.2	13.5	11.26	11.25
8	194491.	22817	873.4	5.992	13.3	13.5	9.212	9.207
9	181960.5	21591.5	877.4	5.880	12.9	13.2	9.052	9.042
10	285502.5	34264	881.4	9.792	12.4	12.8	15.10	15.08
11	259005	31925.5	885.5	1.047	10.7	11.4	16.23	16.20
12	185566	21150.5	889.6	7.560	10.8	10.6	11.72	11.72
13	1162732	136588	426.1	6.700	9.6	9.7	10.43	1.042
14	1445496	170606.5	419.3	9.068	8.5	8.7	14.16	14.15
15	1268031.5	150373.5	413.1	8.404	7.9	8.0	13.16	13.15
16	1068839.5	127776	407.4	6.872	7.9	8.2	10.75	10.74
17	1239790.5	146593.5	399.7	8.664	7.0	7.2	13.60	13.59
18	1353468.5	162350	393.4	1.093	5.9	6.1	17.21	17.20
19	1016468	123165	387.8	8.464	5.6	5.8	13.34	13.33
20	959632.5	114058.5	382.2	8.592	5.1	5.2	13.57	13.56
21	844256	101790	376.6	9.752	3.8	4.0	15.46	15.45
22	686385.5	81292.5	371.7	1.014	2.9	3.0	16.12	16.12
23	540033.5	64208	367.0	1.475	1.6	1.6	23.56	23.55
Standard	318928	36921.5	356.8	0.1 mg Mn				

DATA

Run #12

Solid solution concentration = 75 wt. % MnO-25 wt. % MgO

Cross-sectional area crystal = 1.38 x 1.336 cm^2

Diffusion time = 59 hours 20 minutes

Diffusion temperature = 1300 5°C Glow bar broke before completion

Section number	Counts in peak 0.845 MeV	Counts in peak 1.81 MeV	Decay time minutes	Weight section Mg	Wt. % MnO 0.845 MeV	Wt. % MnO 1.81 MeV	Thickness section 0.845 MeV	Thickness section 1.81 MeV
1	184792	21062	630.8	1.064	25.7	25.6	1.467	1.468
2	541023	63487.5	635.3	4.020	20.4	20.8	5.647	5.637
3	641812.5	76554	640.0	5.488	18.1	18.8	7.769	7.749
4	655689.5	76838	645.5	5.988	17.3	17.7	8.497	8.486
5	620447	73889	650.5	5.868	17.1	17.8	8.333	8.314
6	524828.5	62498	655.6	5.028	17.3	18.0	7.136	7.120
7	786653	93769.5	660.4	8.088	16.5	17.1	11.51	11.49
8	556877.5	65885.5	665.6	5.960	16.2	16.7	8.490	8.475
9	539298.5	64243.5	670.5	6.200	15.4	16.0	8.855	8.837
10	540089	64338.5	675.5	6.384	15.3	15.9	9.120	9.102
11	844606	100121.5	680.6	10.35	15.1	15.6	14.80	14.77
12	702170	94673.5	685.8	10.52	14.3	14.9	15.08	15.05
13	516769	61292	691.0	7.304	13.7	14.2	10.49	10.47
14	608886.5	72817	696.0	9.464	12.8	13.3	13.64	13.61
15	643391	76709	701.0	10.47	12.5	13.0	15.10	15.07
16	478478	56827.5	705.9	9.048	11.0	11.4	13.11	13.10
17	413649.5	49615	711.1	8.352	10.5	11.0	12.12	12.10
18	636065	75921.5	716.0	14.54	9.5	9.9	21.17	21.15
19	429988	48630	721.2	11.32	8.4	8.5	16.54	16.54
20	365819	42953	726.0	12.46	6.7	6.8	18.31	18.30
21	261929.5	31258	730.6	11.50	5.3	5.5	16.98	16.97
22	243986.5	29968.5	736.7	16.11	3.6	3.9	23.91	23.89
23	121495.5	14500.5	741.3	15.40	1.9	2.0	22.98	22.98
Standard	196565.5	22515	449.1	0.1 mg Mn				

XIII. APPENDIX B EXPERIMENTAL EQUIPMENT

Equipment	Make	Model	Serial no.
Ge(Li) detector	ORTEC	8201-0335	9-P421
NaI(Tl) detector	Harshaw	12S12	DE354
Master control	Nuclear Data	2200	67-168
Analog to digital	Nuclear Data	2200	67-232
Reduce/Integrate unit	Nuclear Data		67-4
Memory	Nuclear Data		67-141
Preamp, amplifier and descriminator	Nuclear Data	520	66-204
High voltage power supply	Nuclear Data	537	67-39
Preamp	ORTEC	118A	6255
Amplifier	ORTEC	451	42
6V power supply	Nuclear Data		67-147
High voltage power supply	Burgess Batteries	U-200	
Teletype drive	Nuclear Data		67-33
Tape transport	Nuclear Data		67-13
Output typewriter and paper tape punch	Teletype	33TC	129743
Oscilliscope	Hewlett Packard	H77-120B	601-1140
Cahn electrobalance	Ventron Instruments Corp.	G-2	
Sectioning device (phonograph turntable)	Collara	4TR-200	